THE UNIVERSITY OF MICHIGAN
COLLEGE OF LITERATURE, SCIENCE, AND THE ARTS
Department of Physics

Technical Report No. 3

AN EXPERIMENTAL DETERMINATION OF THE
SPIN EXCHANGE CROSS SECTION OF K^{39} AND Cs^{133}

Thomas E. Stark

ORA Project 04941

under contract with

U. S. ATOMIC ENERGY COMMISSION
CHICAGO OPERATIONS OFFICE
CONTRACT NO. AT(11-1)-1112
ARGONNE, ILLINOIS

ACKNOWLEDGMENTS

TABLE OF CONTENTS

LIST OF TABLES

LIST OF FIGURES

ABSTRACT

An important parameter in many optical pumping experiments is the cross section for spin-exchange collisions. These cross sections measure the probability for interchange of spin coordinates by two electrons in the course of a collision. The accurate determination of these cross sections by optical pumping technique is hampered by inexact knowledge of the atom density in an optical pumping cell.

This thesis reports a value for the exchange cross section for collisions between potassium atoms (K^{39}). The measurements employ the standard techniques of electron paramagnetic resonance (EPR). A microwave absorption spectrum is obtained by observing magnetic dipole transitions between various magnetic sublevels of the ground state of a potassium atom, split by the hyperfine and Zeeman interactions. The spin-exchange collision rate is found by measuring the line widths of isolated transitions and the alkali density determined from an absolute calibration of the microwave spectrometer. For the latter measurement, small weighed-out crystals of copper sulphate, $CuSO_4 \cdot 5H_2O$, are used as standards of intensity.

The role of spin-exchange collisions as a broadening mechanism for magnetic dipole transitions is examined by means of the density matrix formalism. A suitable equation of motion for the density matrix is established and solutions appropriate to the Paschen-Back region of the Zeeman interaction are obtained. Expressions are obtained for the imaginary part of the complex susceptibility, which is related to the microwave power absorbed by the potassium atoms, and for the contributions of spin-lattice and spin-spin relaxation to the observed line width.

The spin-exchange cross sections for collisions between K^{39} atoms is 1.45×10^{-14} cm^2, with an assigned probable error of $\pm 20\%$.

Also reported in this thesis is a value for the exchange cross section for cesium (Cs^{133}). In the case of cesium the hyperfine coupling is sufficiently strong that the Paschen-Back region is not reached for magnetic fields corresponding to the use of X-band microwaves. This is the so-called intermediate field case and results in appreciable mixing of the electron spin states by the hyperfine interaction. Certain corrections in the density matrix treatment follow thereby and are discussed in an appendix.

The measured value of the exchange cross section for Cs^{133} is 2.2×10^{-14} cm^2, with an assigned probable error of $\pm 20\%$.

CHAPTER I

INTRODUCTION

Certain features of the scattering of one-electron atoms were studied in the precise experiments of Wittke and Dicke[1] on the hyperfine structure splitting of atomic hydrogen. Following a suggestion by Purcell, these authors showed that the broadening effects of electron spin exchange collisions placed an effective lower limit on the line width of hyperfine transitions observed in their experiment. At about the same time Purcell and Field[2,28] examined the question of spin exchange broadening for possible astrophysical importance. A classical but surprisingly accurate model for the exchange cross section was also provided.

Later, the effectiveness of spin exchange collisions in transferring spin polarization was exploited by Dehmelt,[3] who succeeded in polarizing free electrons via exchange collisions with optically pumped sodium vapor. Subsequent to this work, other investigators were able to extend the optical pumping technique[4] to a variety of atomic species for which sources of resonance radiation were not conveniently available. A partial listing of these efforts is given in the references.[5]

Additional interest in atomic collision processes accrued with the development of gaseous frequency standards and maser devices. Here again, exchange collisions were shown to have small but easily measurable

effects, not only broadening the transitions but also introducing

secular perturbations which shift the center of the spectral line.

The relationship between exchange collisions and frequency shifts

seems to have been first pointed out by Bender.[6] More recently, ex-

change collisions have been found to play a significant role in the

operation of the hydrogen maser.[7] Frequency shifts attributable to

exchange collisions have also been measured in the optically pumped

rubidium-electron system.[8]

Attempts to characterize spin-exchange collisions by means of an

effective cross section have been hampered by inexact knowledge of the

atom density.* In the case of alkali-alkali cross sections determined

by optical pumping methods, early experimenters relied on vapor pres-

sure data,[9] determining the density of the alkali metal vapor by

measuring the temperature of their optical pumping cells. The resultant

cross sections were in error by as much as a factor of three.[10]

The first accurate measurements of spin exchange cross sections

were reported by Jarrett[11] and Moos[12] in their thesis work at The

University of Michigan. Jarrett combined standard optical pumping

techniques with a scanning Fabry-Perot interferometer to obtain spectral

profiles of the light transmitted by an alkali vapor cell. From these

measurements the integrated absorption coefficient was determined.

---

*In an optical pumping experiment, as in the experiments reported here,
the exchange cross section Q_x cannot be measured directly. What is
measured is the effective rate of exchange, related to Q_x by the formula
$1/T_x = NQ_x\bar{v}$, where N is the atom density and $\bar{v}$ a relative velocity.

Knowledge of the lifetime of an alkali atom in the excited (^2P) state

allowed the density to be calculated. The relation between optical

pumping signal strengths and the effective exchange collision rate was

found by solving the usual rate equations.[6,11] The measurements were

carried out on a mixture of Rb^{85} and Rb^{87}, present in their natural

abundance ratio.

The approach developed by Moos and Sands[13] forms the basis for the

experiments reported in the present work, and we shall on numerous

occasions refer to Moos' thesis[12] for details. Briefly, the experimen-

tal method is that of electron paramagnetic resonance. An absorption

spectrum is obtained by observing magnetic dipole transitions between

various magnetic sublevels of the ground state of an alkali atom, split

by the hyperfine and Zeeman interactions. The spin exchange collision

rate is found by measuring the line widths of isolated transitions and

the alkali density determined from an absolute calibration of the micro-

wave spectrometer.

This method differs in several important respects from the usual

optical pumping schemes:

1. The experiments are conducted at much higher temperatures, and
   correspondingly higher densities. However, the alkali-alkali
   exchange cross sections have been shown to have a rather weak
   temperature dependence so that a meaningful comparison between
   experiments can be made.

2. A source of "pumping" radiation is not required (nor would it
   serve any purpose at the relatively high densities used). Con-
   sistent with the higher operating temperatures the microwave
   resonance technique is sufficiently sensitive to detect transi-
   tions between states whose populations differ only by the

Boltzmann factor. Under these circumstances the relationship between signal strength and exchange rate is relatively simpler than in the case of optical pumping.

3. The measurements are made without the use of a buffer gas and in relatively strong ($\sim$3000 gauss) magnetic fields. Individual transitions are well resolved and no simplifying assumptions need be made as to the degree of excited state mixing caused by gaseous diluents (6^a).

4. Finally, convenient intensity standards can be found which serve to calibrate the spectrometer absolutely in terms of atoms per unit volume. In the present experiment small weighed-out crystals of copper sulphate, $CuSO \cdot 5H_2O$, were used for this purpose.

The remainder of this thesis is ordered as follows. Chapter II is devoted to a theoretical understanding of the spin exchange process. By means of a density matrix formalism the role of exchange collisions in determining spectral line-widths and effective relaxation rates is examined. The question of intermediate field coupling is treated in the Appendix. In Chapter III the experimental apparatus is discussed briefly and the results of the measurements are described.

CHAPTER II

THEORY

A. DYNAMICAL BASIS FOR SPIN EXCHANGE

The dynamical basis for spin exchange between one electron atoms

may be conveniently discussed from the point of view of the Heitler-London

theory of homonuclear diatomic molecules. As a preface to the density

matrix calculations which appear in section B of this chapter, and in

order to introduce the cross section for spin exchange, the nature of

the scattering of alkali metal atoms is discussed.

At large separation the alkali atoms are described by appropriate

atomic orbitals $U_A(1)$ and $U_B(2)$, respectively. Here 1 and 2 are labels

for the electrons and U_A for example, is a hydrogen like wave function

centered on nucleus A. As the two atoms are slowly brought together an

interaction H_{12} is turned on. So long as the interaction is symmetric

in the electron coordinates (i.e., $H_{12}=H_{21}$), any linear combination of

products $U_A(1)\, U_B(2)$ and $U_A(2)\, U_B(1)$ can be used to describe the system,

the only requirement being that the total wave function at most change

sign upon interchange of electrons. Thus, 0th order wave functions for

this problem are

and

$$\psi^s = N^s \left\{ U_A(1) U_B(2) + U_A(2) U_B(1) \right\}$$

$$\psi^A = N^A \left\{ U_A(1) U_B(2) - U_A(2) U_B(1) \right\}$$

(II.1)

5

Here, N^S and N^A are normalization factors which take into account deviations from orthogonality. They are given by

$$N^S = (2 + 2L)^{-1/2}$$

$$N^A = (2 - 2L)^{-1/2} \tag{II.2}$$

where $L = \int U_A(1)U_B(1)U_A(2)U_B(2)d\tau_1 d\tau_2$ measures the overlap in the electron clouds. The energy of interaction as a function of internuclear separation is computed in 1st order using ψ^S and ψ^A as 0th order wave functions and treating H_{12} as a perturbation. The result is

$$V^S(R) = 2E_o + \frac{K+J}{1+L}$$

$$V^A(R) = 2E_o + \frac{K-J}{1-L} \tag{II.3}$$

where $K = \int U_A(1)U_B(2)H_{12}U_A(1)U_B(2)d\tau_1 d\tau_2$ and $J = \int U_A(1)U_B(2)H_{12}U_A(2)U_B(1)d\tau_1 d\tau_2$ are the Coulomb and exchange integrals, respectively.

As yet no mention has been made of the electron spin, and indeed since the interaction is wholly electrostatic the spin plays no direct role. However, the Pauli Exclusion Principle requires that the total wave function, including spin, be antisymmetric in the electron coordinates. Accordingly, the molecular state associated with $V^S(R)$ is $^1\Sigma$ (anti-parallel spins) and with $V^A(R)$, $^3\Sigma$ (parallel spins).

Calculations of the sort described above have been carried out by Rosen and Ikehara[14] for hydrogen and the alkali metals. Hydrogenic atomic orbitals with effective n, Z were used and the integrals J, K, L given in graphical form. The interaction Hamiltonian was taken to be

$$\mathcal{H}_{12} = \frac{e^2}{R} + \frac{e^2}{r_{12}} - \frac{e^2}{r_{1B}} - \frac{e^2}{r_{2B}} \qquad \text{(II.4)}$$

The qualitative form of the interaction potentials is shown in Fig. 1, showing the typical repulsive character of the $^3\Sigma$ state and the tendency of the $^1\Sigma$ state to form stable molecules. From their numerical work, Rosen and Ikehara computed the molecular dissociation energy and equilibrium internuclear separation. Comparison with experimental values was judged to be excellent, tending to support the claim that the main features of the potentials were given by theory, at least for small separation of the atoms.

The significance of the potentials V^S and V^A for the scattering of one electron atoms lies in the very different boundary conditions they impose on the scattering process. Depending on the orientation of the electron spins, the atoms will scatter from one or the other, or both, of these potentials. From the point of view of the Faxen-Holtsmark theory,[16] different scattering cross sections result from the different phase shifts introduced into the scattered wave by these potentials.

To see how the possibility of spin exchange collisions arises, consider two well-separated alkali atoms and assume that the (outer) electrons be found with equal probability in any one of the spin states

$$\chi^{(i)}(1,2) = \begin{cases} \alpha(1)\,\alpha(2) \\ \alpha(1)\,\beta(2) \\ \beta(1)\,\beta(2) \\ \beta(1)\,\alpha(2) \end{cases}$$
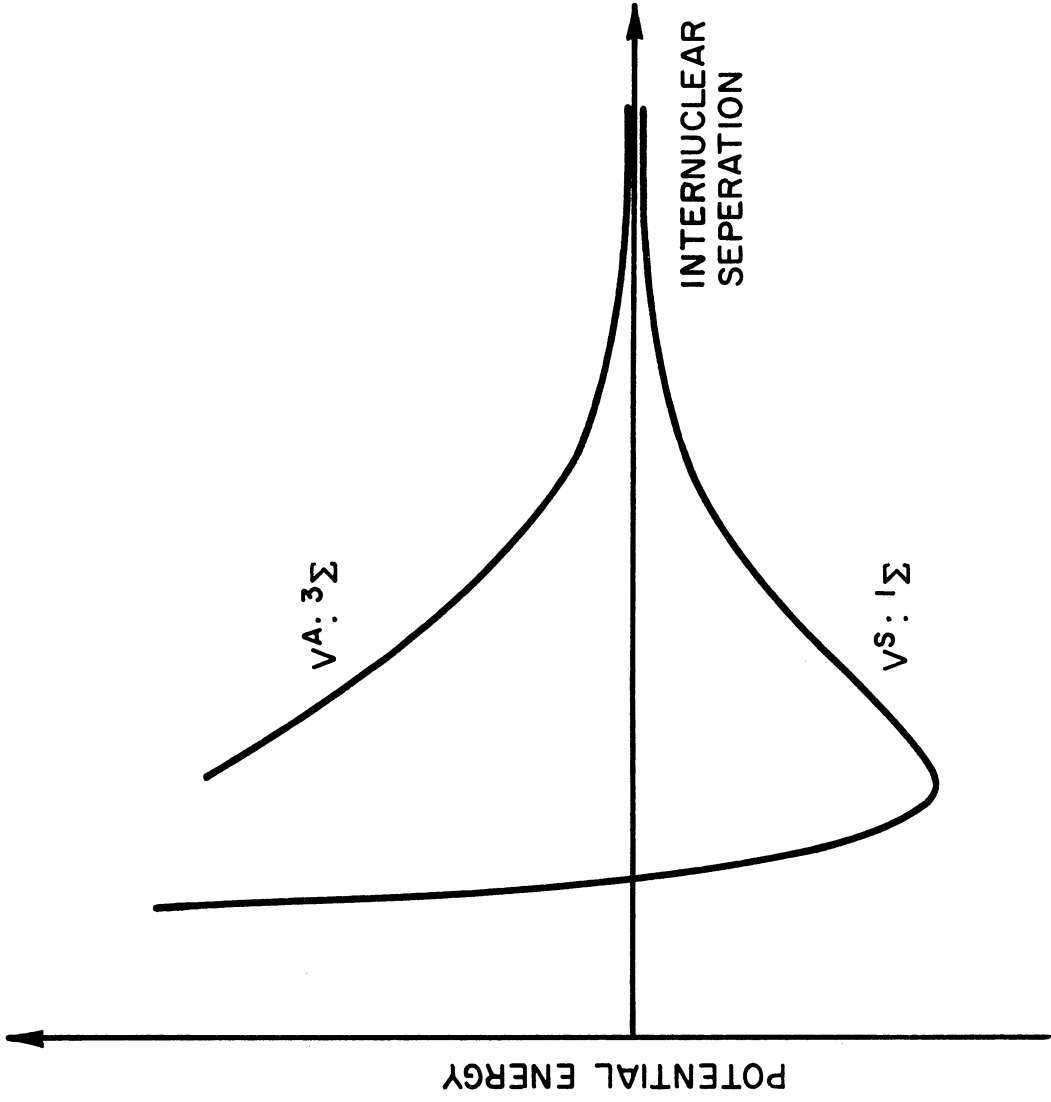
Fig. 1. Molecular potentials in the Heitler-London approximation.

where α and β are the usual spin-up, spin-down functions. If U(1) and U(2) are spatial wave functions for these electrons, a properly (anti) symmetrized wave function describing the pair of atoms at infinite separation (or time $t = -\infty$) is

$$\psi^{(i)} = \frac{1}{\sqrt{2}} \left\{ U(1)U(2)\chi^{(i)}(1,2) - U(2)U(1)\chi^{(i)}(2,1) \right\} .$$ (II.6)

In terms of the functions ψ^S and ψ^A of (II.1), and the spin functions $\chi_S^{(i)} = 1/\sqrt{2} [\chi^{(i)}(1,2)+\chi^{(i)}(2,1)]$, $\chi_A^{(i)} = 1/\sqrt{2} [\chi^{(i)}(1,2)-\chi^{(i)}(2,1)]$, we may rewrite (II.6) in the form

$$\psi^{(i)} = \frac{1}{\sqrt{2}} \left\{ \psi^S \chi_A^{(i)} + \psi^A \chi_S^{(i)} \right\} .$$ (II.7)

Due to the different potential functions V^S and V^A, the spatial parts, ψ^S and ψ^A, evolve differently in time as the two atoms approach and recede from one another. Depending on the values of the angular momentum ℓ and <u>relative</u> kinetic energy $\hbar^2 k^2 = 2\mu E$, where μ is the reduced mass, the phase shifts introduced into the scattered wave function are given by

$$\eta_\ell^S(k) = \frac{1}{\hbar} \int_{-\infty}^{+\infty} V^S(R) \, dt$$

and (II.8)

$$\eta_\ell^A(k) = \frac{1}{\hbar} \int_{-\infty}^{+\infty} V^A(R) \, dt ,$$

respectively. Thus, after the collision and when the atoms are again at infinite separation (or time $t = +\infty$), the wave function for the pair can be written

$$\psi_c^{(i)} = \frac{1}{\sqrt{2}}\left\{ e^{i\varphi_\ell^S(k)}\psi^S\chi_A^{(i)} + e^{i\varphi_\ell^A(k)}\psi^A\chi_S^{(i)} \right\} \qquad \text{(II.9)}$$

Considering only relative phase changes, (II.9) may be written in the form of Eq. (II.6) with the result

$$\psi_c^{(i)} = \frac{1}{2}\left[e^{i\varphi_\ell(k)} + 1 \right] \times \frac{1}{\sqrt{2}}\left\{ u(1)u(2)\chi^{(i)}(1,2) - u(2)u(1)\chi^{(i)}(2,1) \right\}$$

$$+ \frac{1}{2}\left[e^{i\varphi_\ell(k)} - 1 \right] \times \frac{1}{\sqrt{2}}\left\{ u(1)u(2)\chi^{(i)}(2,1) - u(2)u(1)\chi^{(i)}(1,2) \right\}$$

$$\equiv \frac{1}{2}\left[e^{i\varphi_\ell(k)} + 1 \right]\psi^{(i)} + \frac{1}{2}\left[e^{i\varphi_\ell(k)} - 1 \right]\psi_x^{(i)} \qquad \text{(II.10)}$$

where

$$\varphi_\ell(k) \equiv \varphi_\ell^A(k) - \varphi_\ell^S(k) \qquad \text{(II.11)}$$

Note that the second term, $\psi_x^{(i)}$, differs from the first only in the interchange of electron __spin__ coordinates. The probability that in a collision such a spin exchange takes place is given by

$$\left| \left(\psi_x^{(i)}, \psi_c^{(i)} \right) \right|^2 = \sin^2 \frac{\varphi_\ell(k)}{2} \qquad \text{(II.12)}$$

These results may be succinctly summarized by introducing the Dirac exchange operator $P_{12} = 1/2\,(1+\vec{\sigma}_1\cdot\vec{\sigma}_2)$, where the σ's are the usual Pauli matrices. Then $\psi_x^{(i)} = P_{12}\,\psi^{(i)}$ and

$$\psi_c^{(i)} = \left\{ \frac{1}{4}\left(3e^{i\varphi_\ell(k)} + 1\right) + \frac{1}{4}\left(e^{i\varphi_\ell(k)} - 1\right)\vec{\sigma}_1\cdot\vec{\sigma}_2 \right\}\psi^{(i)}$$

$$\equiv M_\ell(k)\,\psi^{(i)} \qquad \text{(II.13)}$$

The results obtained so far pertain only to the scattering of the ℓth partial wave for two atoms of relative energy $E = \hbar^2 k^2/2\mu$. The quantities

$$f_\ell^d \equiv \tfrac{1}{4}\left(3 e^{i\,\phi_\ell(k)} + 1\right)$$

and

$$f_\ell^x \equiv \tfrac{1}{4}\left(e^{i\,\phi_\ell(k)} - 1\right)$$

(II.14)

may be interpreted as the "direct" and "exchange" __partial__ scattering amplitudes, respectively. In terms of them, Eq. (II.10) and (II.13) may be written

$$\psi_c^{(i)} = \left(f_\ell^d - f_\ell^x\right)\psi^{(i)} + 2 f_\ell^x \psi_x^{(i)}$$

(II.10a)

$$\psi_c^{(i)} = \left\{ f_\ell^d + f_\ell^x \,\vec{\sigma}_1 \cdot \vec{\sigma}_2 \right\} \psi^{(i)}$$

(II.13a)

In the Faxen-Holtsmark theory the scattering amplitudes of the various partial waves are linearly superposed[17] yielding

$$F_d(\Theta) = \tfrac{1}{k} \sum_{\ell=0}^{\infty} (2\ell+1)\, f_\ell^d \, P_\ell(\cos\Theta)$$

(II.15)

$$F_x(\Theta) = \tfrac{1}{k} \sum_{\ell=0}^{\infty} (2\ell+1)\, f_\ell^x \, P_\ell(\cos\Theta)$$

Thus, an immediate generalization of (II.13) is

$$\psi_c^{(i)} = M(k)\,\psi^{(i)}$$

where $M(k) = F_d(\Theta) + F_x(\Theta)\,\vec{\sigma}_1 \cdot \vec{\sigma}_2$. The total cross section for spin exchange is then

$$Q_x = 2\pi \int |F_x(\Theta)|^2 \, d(\cos\Theta)$$

(II.16)

$$= \frac{\pi}{k^2} \sum_{\ell=0}^{\infty} (2\ell+1) \sin^2 \frac{\phi_\ell(k)}{2}$$

and comparison with the usual expression for this cross section[17] shows

that

$$Q_\ell(k) \equiv 2 \left[\delta_\ell^1(k) - \delta_\ell^0(k) \right]$$

where δ_ℓ^1 and δ_ℓ^0 are the quantum mechanical phase shifts for scattering

from the spherically symmetric triplet (V^A) and singlet (V^S) potentials,

respectively. For the purposes of this paper, the operator $M_\ell(k)$ is more

convenient and will be used in subsequent calculations.

B. EQUATION OF MOTION FOR THE DENSITY MATRIX

A detailed examination of the role of spin exchange collisions in

determining the lifetime of an electron in a given spin state follows.

To facilitate the interpretation of the experimental results a model is

required on which to base the observations. The treatment of spin ex-

change given here follows the discussion of Wittke and Dicke[1] on this

same problem. The objective of the calculation is to establish a rela-

tionship between observed spectral line width and the cross section for

spin exchange.

Since the details of the motion of the atomic spins are of primary

interest, rather than the gross deflections of the atoms themselves, it

will be sufficient to regard the atoms as being in definite but unspeci-

fied states of relative momentum before and after the collision. Atten-

tion may be confined to the atomic spins, taking into account their

statistical character by means of the density matrix formalism.[18]

Furthermore, in so far as it is improbable that successive collisions

would involve the same pair of atoms, the atoms may be regarded as statistically independent and hence uncorrelated.

Consider, then, two alkali atoms, chosen at random from an assembly of N such atoms, and presumed about to collide. The density matrices used to describe the incoming atoms are obtained as follows. Let ψ_1 and ψ_2 be the (total) spin functions for atoms 1 and 2, respectively. These can be expanded in terms of spin functions $|i\rangle$, which are used to label the rows and columns of the density matrix. Thus

$$\psi_1 = \sum_i a_i^{(1)} |i\rangle \qquad\qquad \psi_2 = \sum_i a_i^{(2)} |i\rangle$$

and the corresponding density matrices are given by

$$(\rho_1)_{ij} = a_i^{(1)} a_j^{(1)*} \qquad\qquad (\rho_2)_{ij} = a_i^{(2)} a_j^{(2)*}$$

With the assumption that the atoms are not correlated by previous collisions, the wave function for the combined system prior to a collision is

$$\psi_{12} = \psi_1 \psi_2 = \sum_{i,j} a_i^{(1)} a_j^{(2)} |i,j\rangle$$

so that the density matrix for the pair is

$$(\rho_{12})_{ij,k\ell} = a_i^{(1)} a_j^{(2)} \left(a_k^{(1)} a_\ell^{(2)} \right)^*$$

$$= (\rho_1)_{ik} (\rho_2)_{j\ell}$$

(II.17)

In matrix notation $\rho_{12} = \rho_1 \otimes \rho_2$, where the symbol $\otimes$ denotes the direct, or outer product of the matrices ρ_1 and ρ_2.

According to section A of this chapter, the wave function for this
pair of atoms after a collision is given by

$$\psi_{12}^{c} = M_{\ell}(k)\, \psi_{12}$$

Therefore, after the collision the pair of atoms is described by the
density matrix

$$\rho_{12}^{c} = M_{\ell}(k)\, \rho_{12}\, M_{\ell}(k)^{*} \qquad\qquad (\text{II}.18)$$

Finally, the density matrix for one of the atoms is recovered by taking

the trace over ρ_{12}^{c} with respect to all quantities bearing the indices

of the other atom. Thus

$$\rho_{1}^{c} = TR_{(2)}\, \rho_{12}^{c} = TR_{(2)}\, M_{\ell}(k)\, \rho_{12}\, M_{\ell}(k)^{*}$$

$$\rho_{2}^{c} = TR_{(1)}\, \rho_{12}^{c} = TR_{(1)}\, M_{\ell}(k)\, \rho_{12}\, M_{\ell}(k)^{*}$$

With some labor the operator M (Eq. II.13) may be substituted in these

equations with the result that

$$\begin{aligned}
\left(\rho_{1}^{c}\right)_{ij} &= \tfrac{1}{4}\left(4 - 3\sin^{2}\tfrac{\ell}{2}\right)\left(\rho_{1}\right)_{ij} + \tfrac{1}{4}\sin^{2}\tfrac{\ell}{2}\sum_{\beta}\langle i|\sigma_{\beta}\rho_{1}\sigma_{\beta}|j\rangle \\
&+ \tfrac{1}{16}\left(1 - e^{i\ell}\right)\left(3 + e^{-i\ell}\right)\sum_{\beta}\langle i|\sigma_{\beta}\rho_{1}|j\rangle\, TR_{(2)}[\sigma_{\beta}\rho_{2}] \\
&+ \tfrac{1}{16}\left(1 - e^{-i\ell}\right)\left(3 + e^{i\ell}\right)\sum_{\beta}\langle i|\rho_{1}\sigma_{\beta}|j\rangle\, TR_{(2)}[\sigma_{\beta}\rho_{2}] \qquad (\text{II}.19)\\
&- \tfrac{i}{4}\sin^{2}\tfrac{\ell}{2}\sum_{\alpha}\left\{\langle i|\sigma_{\alpha}\rho_{1}\sigma_{\beta}|j\rangle - \langle i|\sigma_{\beta}\rho_{1}\sigma_{\alpha}|j\rangle\right\} \times \\
&\times TR_{(2)}[\sigma_{\gamma}\rho_{2}]
\end{aligned}$$

using the fact that $TR(1)\rho_1 = TR(2)\rho_2 = 1$ and allowing, in the last

term, $\alpha\beta\gamma$ to form a cyclic permutation of XYZ. For simplicity, the

labels on $\varphi_{\ell}(k)$ have been dropped.

As an example of the use of Eq. (II.19) consider a single scattering event between two "nonequivalent" spin-1/2 particles. For the states $|i\rangle$ take the usual spin up, spin down functions α and β. Suppose that particle 1 has been prepared, in some way, so that it is entirely in the spin up state α. The density matrix for this particle is then

$$\rho_1 = \begin{pmatrix} 1 & 0 \\ 0 & 0 \end{pmatrix}$$

On the other hand, suppose that particle 2 is thermal; that is, there is a Boltzmann distribution among the states α, β. Then

$$\rho_2 = \begin{pmatrix} \rho_{11}^0 & 0 \\ 0 & \rho_{22}^0 \end{pmatrix}$$

with $\rho_{11}^0 + \rho_{22}^0 = 1$. The polarization of these particles is given by $Z = TR(\sigma_i \rho)$ so that $Z_1 = 1$ and $Z_2 = Z_2^0 = \rho_{11}^0 - \rho_{22}^0$. To find the density matrices after a single collision apply Eq. (II.19). The result is, for the polarizations,

$$Z_1^c = 1 - \left(1 - Z_2^0\right) \sin^2 \frac{\theta}{2}$$

$$Z_2^c = 1 - \left(1 - Z_2^0\right) \cos^2 \frac{\theta}{2}$$

An important conclusion to be drawn from this example is that although exchange collisions rearrange the populations of the spin states and hence alter the polarization, the total polarization $Z_1 + Z_2 = Z_1^c + Z_2^c$. That is, exchange collisions act as a sort of relaxation mechanism for the state populations, but not in the sense in which relaxation is generally understood: spin exchange collisions do not dissipate the total (spin) angular momentum of the system.

So far only the effects of a single exchange collision have been considered as a possible mechanism of change for the density matrix. To find the average effect of many such collisions, acting in competition with other types of collisions and with externally applied driving forces, it is necessary to find, and solve, an appropriate equation of motion for the density matrix. Such an equation of motion will be obtained by following the procedure of Karplus and Schwinger.[19]

Assuming that the atomic gas is sufficiently rare, and the collision cross sections sufficiently small, collisions occur with a mean frequency $1/\tau_c$ where τ_c, the mean time between collisions, is long compared to the time t_c of a collision. Let ρ be the density matrix for a representation atom in the gas. Except for a small time interval $\sim t_c$ the density matrix is free to evolve in time according to the usual equation of motion.[18]

$$i\hbar\frac{\partial\rho}{\partial t} = [H,\rho]$$
(II.20)

where H is the spin Hamiltonian including externally applied fields if any. Furthermore, if t_c is short compared with the characteristic periods of the Hamiltonian, changes in ρ due to H during the collision itself may be ignored. Thus a single collision has the effect of providing an initial condition to the solution of Eq. (II.20). If t_0 is the time of the last collision the density matrix will at all later times depend at least parametrically on t_0. Formally, the solution can be written as $\rho(t,t_0)$, where $\rho(t_0,t_0) \equiv \rho_c$ is the initial value of the

density matrix. The form of ρ_c defines the type of collision that has occurred.

To find the effect of many collisions an average over the distribution of collision times t_0 is taken:

$$\bar{\rho}(t) = \int_{-\infty}^{t} \rho(t,t_0)\, P(t_0)\, dt_0 \tag{II.21}$$

where $P(t_0)dt_0$ is the probability that the last collision occurred in the interval t_0 to $t_0 + dt_0$. For collisions which occur randomly at a mean rate $1/\tau_c$,

$$P(t_0)dt_0 = \frac{1}{\tau_c} e^{-(t-t_0)/\tau_c}\, dt_0 \tag{II.22}$$

To find the equation of motion satisfied by $\bar{\rho}(t)$ we differentiate Eq. (II.21), using Leibnitz rule, and Eq. (II.20), to find

$$\frac{\partial \bar{\rho}}{\partial t} = -\frac{i}{\hbar}[H,\bar{\rho}] - \frac{1}{\tau_c}(\bar{\rho} - \rho_c) \tag{II.23}$$

In the case of spin exchange collisions ρ_c is given by Eq. (II.19) and $1/\tau_c = \sqrt{2}NQ_c^{\ell}\bar{v}$. N is the number of atoms per unit volume, $\bar{v}$ the average speed. Q_c^{ℓ} will be taken to be $\pi/k^2(2\ell+1)$, the maximum partial cross section associated with the turning on of the exchange operator $f_{\ell}^{x}\,\vec{\sigma}_1 \cdot \vec{\sigma}_2$. Seemingly little justification for this choice can be made, except that it be noted that the "direct" amplitude f_{ℓ}^{d} does not contribute to scattering in which the spin state changes.[27] In this work only those states are observed in which such a spin change occurs. However, we cannot set $f_{\ell}^{d}=0$, for it will be seen later that the inter-

ference of the "direct" and "exchange" amplitudes leads to a frequency shift.[6,8] Since the operator M_ℓ admits of the possibility that in a given collision no exchange occurs, Q_c^ℓ cannot be identified with the exchange cross section.

Spin exchange does not provide a mechanism for restoring thermal equilibrium to a spin system. Energy added to the spin system by external fields cannot reappear at the walls of the container but rather is distributed by collisions in such a way as to equalize the populations of all the levels. In order to allow for relaxation we must specifically include relaxation collisions in the equation of motion. This may be done by repeating the averaging procedure. Relaxation collisions are presumed to occur at a mean rate $1/T_1$, with the initial condition on the density matrix being $\overline{\rho}(t_o,t_o) = \rho_o$. ρ_o is the density matrix describing thermal equilibrium among the spin states at a (kinetic) temperature T. The result is

$$\frac{\partial \rho}{\partial t} = -\frac{i}{\hbar}[H,\rho] - \frac{1}{T_c}(\rho - \rho_e) - \frac{1}{T_1}(\rho - \rho_o) \qquad (II.24)$$

With the Hamiltonian described below, (II.24) is the equation of motion which will be solved.

It should be noted that this equation of motion is only correct where no correlation exists between the process of relaxation and that of spin exchange. No correlation is expected here.

C. SOLUTION TO THE EQUATION OF MOTION

In the presence of a static magnetic field H_O along the Z-axis

and a microwave frequency magnetic field $2H_1\cos\omega t$ along the X-axis, the

Hamiltonian for the alkali atoms is

$$\mathcal{H} = g_s\mu_o H_o S_z - g_I\mu_o H_o I_z + A\vec{I}\cdot\vec{S}$$

$$+ 2\mu_o H_1 \cos\omega t(g_s S_x + g_I I_x) \tag{II.25}$$

$$\equiv \mathcal{H}_o + \mathcal{H}_i(t)$$

where μ_O is the Bohr magneton and A measures the strength of the Fermi

contact interaction (hyperfine interaction). For our problem the terms

proportional to the nuclear g-value are of little interest, since

$g_I \sim 1/2000\ g_S$. Also, $2H_1 \ll H_O$ so that $H_i(t)$ may be treated as a

perturbation.

The eigenvalues of $\mathcal{H}_o$, for S = 1/2 and arbitrary field strengths

H_O, are given by the Breit-Rabi formula[20]

$$E_M^F = \frac{A}{2}\left[I + \frac{2I+1}{2}X\right] \qquad M = I + \tfrac{1}{2}$$

$$= \frac{A}{2}\left[I - \frac{2I+1}{2}X\right] \qquad M = -(I+\tfrac{1}{2}) \tag{II.26}$$

$$= \frac{A}{2}\left[-\tfrac{1}{2} + \frac{2I+1}{2}\sqrt{1+\frac{4M}{2I+1}X + X^2}\right]$$

$$E_M^{F-1} = \frac{A}{2}\left[-\tfrac{1}{2} + \frac{2I+1}{2}\sqrt{1+\frac{4M}{2I+1}X + X^2}\right] \qquad M = (I-\tfrac{1}{2}), \cdots, -(I-\tfrac{1}{2})$$

M is the projection of the total angular momentum on the Z-axis,

$X = 2g_S\mu_o H_o/A(2I+1)$, and $F = I+S$. The corresponding eigenfunctions

(normalized) are easily found to be

$$\psi_M^F = |m_I = I, m_s = +\tfrac{1}{2}\rangle = |I, \tfrac{1}{2}\rangle \qquad M = I + \tfrac{1}{2}$$

$$= |m_I = -I, m_s = -\tfrac{1}{2}\rangle = |-I, -\tfrac{1}{2}\rangle \qquad M = -(I + \tfrac{1}{2})$$

$$= [\Lambda_M^2 + \lambda_M^2]^{-1/2} \left\{ \lambda_M |m_I - 1, \tfrac{1}{2}\rangle + \Lambda_M |m_I, -\tfrac{1}{2}\rangle \right\} \qquad \text{(II.27)}$$

$$\psi_M^{F-1} = [\Lambda_M^2 + \lambda_M^2]^{-1/2} \left\{ -\Lambda_M |m_I - 1, \tfrac{1}{2}\rangle + \lambda_M |m_I, -\tfrac{1}{2}\rangle \right\}$$

$$M = (I - \tfrac{1}{2}), \cdots, -(I - \tfrac{1}{2})$$

where

$$\Lambda_M = -X - \frac{2M}{2I+1} + \sqrt{1 + \frac{4M}{2I+1} X + X^2}$$ (II.27a)

$$\lambda_M = \frac{2}{2I+1} \sqrt{(I + M + \tfrac{1}{2})(I - M + \tfrac{1}{2})}$$

The energy eigenfunctions are used to construct the density matrix

ρ for an alkali atom, the matrix being of dimension $2(2I+1)$. In this

representation ρ_0 is a diagonal matrix, the diagonal matrix elements

being equal to the fractional population of the corresponding energy

states.

A case of particular interest is one for which the microwave fre-

quency is close to the resonant frequency for transitions between a

pair of states. The density matrix will then have off-diagonal matrix

elements corresponding to the excitation of these levels by the microwave

field. Although the spin exchange term in Eq. (II.24) couples this

pair of levels to the remaining levels in the atom, other off-diagonal

matrix elements will be negligible so long as the various transitions

are well-resolved (see Appendix).

The solution of the equation of motion will be examined when the static field is large, so that the Zeeman interaction dominates the hyperfine splitting. For large values of the parameter X the eigenfunctions become simple products of the nuclear and electronic spin functions and the energy levels become linear in the applied field H_0. The selection rules for magnetic dipole transitions are $\Delta M_S = \pm 1$, $\Delta M_I = 0$.

The microwave frequency is assumed near the resonant frequency for transitions between the states $|I, + 1/2\rangle$ and $|I, - 1/2\rangle$. The corresponding off-diagonal matrix elements in ρ will be denoted by ρ_{12} and $\rho_{21} = \rho_{12}^*$. The diagonal elements will be denoted by $\rho_{M_I}^{M_S} \equiv \rho_M^\pm$ $(-I \leq M \leq I)$.

From Eq. (II.19) the matrix elements of ρ_c are

$$(\rho_c)_M^+ = \rho_M^+ - \tfrac{1}{2}(1-z)\sin^2\tfrac{\theta}{2}\,\rho_M^+ + \tfrac{1}{2}(1+z)\sin^2\tfrac{\theta}{2}\,\rho_M^-$$

$$(\rho_c)_M^- = \rho_M^- - \tfrac{1}{2}(1+z)\sin^2\tfrac{\theta}{2}\,\rho_M^- + \tfrac{1}{2}(1-z)\sin^2\tfrac{\theta}{2}\,\rho_M^+$$

$$(\rho_c)_{12} = (\rho_c)_{21}^* = \rho_{12} - \sin^2\tfrac{\theta}{2}\,[1-(\rho_I^+ + \rho_I^-)]\rho_{12}$$
$$-\tfrac{1}{2}\sin\theta\,[z-(\rho_I^+ - \rho_I^-)]\rho_{12}$$

where $Z = \sum_m \rho_m^+ - \sum_m \rho_m^-$; the matrix elements of $[H,\rho]$ are then

$$\langle m, +\tfrac{1}{2}|[H,\rho]|m, +\tfrac{1}{2}\rangle = \langle m, -\tfrac{1}{2}|[H,\rho]|m, -\tfrac{1}{2}\rangle = 0 \qquad m \neq I$$

$$\langle I, +\tfrac{1}{2}|[H,\rho]|I, +\tfrac{1}{2}\rangle = \tfrac{1}{2}g_s\mu_0 2H_1\cos\omega t\,(\rho_{21} - \rho_{12})$$

$$\langle I, -\tfrac{1}{2}|[H,\rho]|I, -\tfrac{1}{2}\rangle = -\tfrac{1}{2}g_s\mu_0 2H_1\cos\omega t\,(\rho_{21} - \rho_{12})$$

$$\langle I, +\tfrac{1}{2}|[H,\rho]|I, -\tfrac{1}{2}\rangle = -\tfrac{1}{2}g_s\mu_0 2H_1\cos\omega t\,(\rho_I^+ - \rho_I^-) + \rho_{12}(E_I^+ - E_I^-)$$

$$\langle I, -\tfrac{1}{2}|[H,\rho]|I, +\tfrac{1}{2}\rangle = \tfrac{1}{2}g_s\mu_0 2H_1\cos\omega t\,(\rho_I^+ - \rho_I^-) - \rho_{21}(E_I^+ - E_I^-)$$

Let $E_I^+ - E_I^- \equiv \hbar\omega_0$, $\gamma \equiv 2\langle i|\mu x|j\rangle/\hbar \equiv g_S\mu_0/\hbar$ and $\gamma H_1 = \omega_1$; then

a)
$$\dot{\rho}_I^+ = -i\omega_1\cos\omega t\,(\rho_{21}-\rho_{12}) - \frac{1}{\tau_c}\left\{\tfrac{1}{2}(1-z)\sin^2\tfrac{\psi}{2}\,\rho_I^+ - \tfrac{1}{2}(1+z)\sin^2\tfrac{\psi}{2}\,\rho_I^-\right\} - \frac{1}{T_1}\left(\rho_I^+ - \rho_I^{+0}\right)$$

b)
$$\dot{\rho}_I^- = +i\omega_1\cos\omega t\,(\rho_{21}-\rho_{12}) - \frac{1}{\tau_c}\left\{\tfrac{1}{2}(1+z)\sin^2\tfrac{\psi}{2}\,\rho_I^- - \tfrac{1}{2}(1-z)\sin^2\tfrac{\psi}{2}\,\rho_I^+\right\} - \frac{1}{T_1}\left(\rho_I^- - \rho_I^{-0}\right)$$

$$(\text{II.28})$$

c,d)
$$\dot{\rho}_{12} = \dot{\rho}_{21}^* = -i\omega_0\rho_{12} + i\omega_1\cos\omega t\,(\rho_I^+ - \rho_I^-) - \frac{1}{T_1}\rho_{12}$$
$$- \frac{1}{\tau_c}\left\{[1-(\rho_I^+ + \rho_I^-)]\sin^2\tfrac{\psi}{2}\,\rho_{12}\right\}$$
$$+ \frac{i}{2}\sin\psi\left[z-(\rho_I^+ - \rho_I^-)\right]\rho_{12}$$

e)
$$\dot{\rho}_m^+ = -\frac{1}{\tau_c}\left\{\tfrac{1}{2}(1-z)\sin^2\tfrac{\psi}{2}\,\rho_m^+ - \tfrac{1}{2}(1+z)\sin^2\tfrac{\psi}{2}\,\rho_m^-\right\} - \frac{1}{T_1}\left(\rho_m^+ - \rho_m^{+0}\right)$$

f)
$$\dot{\rho}_m^- = -\frac{1}{\tau_c}\left\{\tfrac{1}{2}(1+z)\sin^2\tfrac{\psi}{2}\,\rho_m^- - \tfrac{1}{2}(1-z)\sin^2\tfrac{\psi}{2}\,\rho_m^+\right\} - \frac{1}{T_1}\left(\rho_m^- - \rho_m^{-0}\right)$$

where, in Eqs. e) and f), $m \neq I$. Also, Z is the total polarization of the gas and $Z_m = \rho_m^+ - \rho_m^-$ is the partial polarization associated with the pair of states $|M, +1/2\rangle$ and $|M, -1/2\rangle$. From Eqs. e) and f)

$$\dot{z}_m \equiv \dot{\rho}_m^+ - \dot{\rho}_m^- = -\frac{1}{\tau_c}\left\{\sin^2\tfrac{\psi}{2}z_m - \sin^2\tfrac{\psi}{2}z N_m\right\}$$
$$- \frac{1}{T_1}\left\{z_m - z_m^0\right\}$$

$$(\text{II.29})$$

$$\dot{N}_m \equiv \dot{\rho}_m^+ + \dot{\rho}_m^- = -\frac{1}{T_1}\left\{N_m - N_m^0\right\}$$

According to (II.16) the spin exchange partial cross section is

$$Q_X = \sin^2 \frac{\theta}{2} \, Q_c$$

the mean rate for exchange collisions is then

$$\frac{1}{\tau_X} \equiv \frac{\sin^2 \frac{\theta}{2}}{\tau_c} = \sqrt{2} \, N Q_X \overline{\upsilon} \tag{II.30}$$

Substituting into (II.29) and summing over all $M \neq I$:

$$\sum_{m \neq I} \dot{Z}_m = -\frac{1}{\tau_X} \left\{ \sum_{m \neq I} Z_m - Z \sum_{m \neq I} N_m \right\}$$

$$\qquad\qquad - \frac{1}{\tau_1} \left\{ \sum_{m \neq I} Z_m - \sum_{m \neq I} Z_m^0 \right\} \tag{II.31}$$

$$\sum_{m \neq I} \dot{N}_m = -\frac{1}{\tau_1} \left\{ \sum_{m \neq I} N_m - \sum_{m \neq I} N_m^0 \right\}$$

Finally, we substitute for $Z = Z_I + \sum_{m \neq I} Z_m$. In the high temperature

approximation $(kT \gg \vec{\mu} \cdot \vec{H})$ the equilibrium distribution of population is

nearly uniform over the spin states; thus, $N_m^0 \simeq 1/2I+1$ and $Z^0 \simeq (2I+1)$

Z_I^0. The steady state solutions to (II.31) are

$$\sum_{m \neq I} N_m = \sum_{m \neq I} N_m^0 \simeq \frac{2I}{2I+1}$$

$$\sum_{m \neq I} Z_m \simeq \left(\frac{2I}{\tau_1} Z_I^0 + \frac{2I}{2I+1} \frac{1}{\tau_X} Z_I \right) \left(\frac{1}{\tau_1} + \frac{1}{2I+1} \frac{1}{\tau_X} \right)^{-1} \tag{II.32}$$

Using these results the remaining Eqs. a)-d) can be combined to

give

$$\dot{Z}_I \equiv \dot{\rho}_I^+ - \dot{\rho}_I^- = 2\omega_1 \cos \omega t \, Y_I - \frac{1}{\tau_1} \left(Z_I - Z_I^0 \right)$$

$$\dot{X}_I \equiv \dot{\rho}_{12} + \dot{\rho}_{21} = -(\omega_0 + \Delta) Y_I - \frac{1}{\tau_2} X_I \tag{II.33}$$

$$\dot{Y}_I \equiv i(\dot{\rho}_{12} - \dot{\rho}_{21}) = +(\omega_0 + \Delta) X_I - 2\omega_1 \cos \omega t \, Z_I - \frac{1}{\tau_2} Y_I$$

where

$$\frac{1}{T_2} = \frac{1}{T_1} + \frac{2I}{2I+1}\frac{1}{T_x}$$

$$\frac{1}{T_1} = \frac{1}{T_1} + \frac{1}{\frac{1}{2I}T_1 + \frac{2I+1}{2I}T_x}$$

(II.34)

Equations (II.33) may be compared with the well-known Bloch equations of nuclear magnetic resonance theory. There, as here, T_2 is the spin-spin relaxation time responsible for the spectral line width; T_1 is the spin-lattice relaxation time governing the return of a disturbed spin system to thermal equilibrium. The quantity Δ in these equations represents a frequency shift in the line center; Δ is given by

$$\Delta = \frac{1}{2} N\sqrt{2}\,\overline{\upsilon}\,Q_c\,\sin\varphi \sum_{m \neq I}Z_m$$

(II.35)

$$\simeq \sqrt{2}\,N\,\overline{\upsilon}\,I\,Q_c\,\sin\varphi\,Z_I^{\,o}$$

X_I, Y_I and Z_I are, except for multiplicative factors, the components of magnetization of the sample.

The steady state solution to Eqs. (II.33) may be obtained by transforming to a coordinate system which rotates with the frequency of the applied rf magnetic field and in the sense of the Larmor precession of the spins. In doing this certain high frequency nonresonant terms which oscillate like $\cos 2\omega t$ appear in the equations. These terms are due to the counter rotating component of the rf magnetic field, which has been taken to be linearly polarized, and give rise to the Bloch-Siegert

shift of the line center.[21] This effect will be ignored.

The solutions obtained in this way are part of the standard literature on magnetic resonance.[22] In the rotating coordinate system the components of magnetization in phase and out of phase with respect to the microwave field are denoted by u and v, respectively. It is convenient to express the solution in terms of the components of the complex rf susceptibility $\chi_{rf} = \chi' - i\chi''$, where

$$\chi' = -v/2H_1$$

$$\chi'' = +u/2H_1$$

One finds[22]

$$\chi' = \frac{1}{2}\chi_0 \omega_0 \tau_2 \frac{\tau_2(\omega_0 + \Delta - \omega)}{1 + \tau_2^2(\omega_0 + \Delta - \omega)^2 + \gamma^2 H_1^2 \tau_1 \tau_2}$$

$$\chi'' = \frac{1}{2}\chi_0 \omega_0 \tau_2 \frac{1}{1 + \tau_2^2(\omega_0 + \Delta - \omega)^2 + \gamma^2 H_1^2 \tau_1 \tau_2}$$

(II.36)

where χ_0 is the static susceptibility and τ_1 and τ_2 are given by (II.34). The average rate P at which power is absorbed per unit volume by the gas from the microwave field is

$$P = \frac{\omega}{2\pi} \int_0^{\omega/2\pi} \vec{H} \cdot \frac{d\vec{M}}{dt} dt = 2\omega\chi'' H_1^2$$

(II.37)

Although the equations have been derived for a specific pair of spin states, all the results do in fact apply to any other pair of states of the form $|M, \pm 1/2\rangle$. In particular the frequency shift Δ is always in the same direction, determined only by $Z_I^0 \simeq (1/2I+1)Z^0$ and $\sin(\delta_\ell^1 - \delta_\ell^0)$. Since $Z^0 < 0$, measuring the sense of the frequency shift

will also measure the relative values of δ_ℓ^1 and δ_ℓ^0. Unfortunately the very small (thermal) polarization precludes such a measurement in the present case $(\Delta/\omega_0 \sim 10^{-12})$.

Of considerable importance here are the conclusions embodied in Eqs. (II.34), (II.36), and (II.37). As a function of microwave frequency Eq. (II.37) predicts a Lorentzian line shape with half-width at half power points equal to $1/\tau_2$, so long as $\gamma^2 H_1^2 \tau_1 \tau_2 \ll 1$. (The latter quantity is called the saturation factor and can generally be made small by suitable reduction of the microwave power). Through Eq. (II.34) it is clear that both exchange and relaxation contribute to the observed line width. The effective spin lattice relaxation time can be found from a measurement of the saturation factor $\gamma^2 H_1^2 \tau_1 \tau_2$ and the observed line width then corrected. The effectiveness of spin exchange in coupling a given pair of levels to the remaining levels of the system is illustrated in Fig. 2, where τ_1/τ_2, the measured variables, are plotted versus T_1/T_x, the variables of physical interest. Eq. (II.34) may also be interpreted through the electrical network analogue shown in Fig. 3.

It should be noted that broadening effects due to unavoidable field inhomogeneities are not included in Eq. (II.34). The effect of an inhomogeneous dc field (H_0) may be included by defining

$$\frac{1}{\tau_2'} = \frac{1}{\tau_2} + \frac{1}{\tau_2^*} \qquad \qquad (II.38)$$
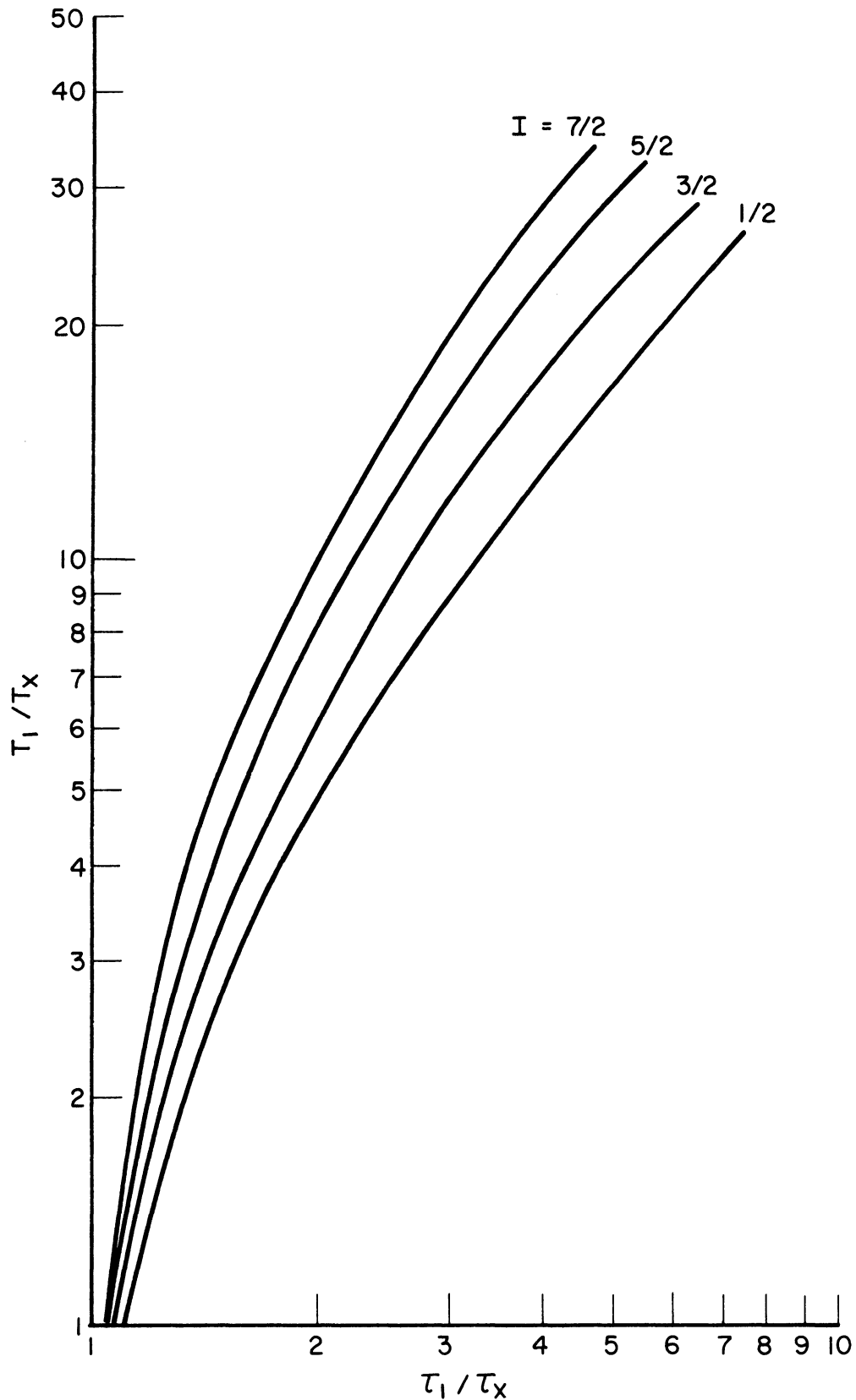
Fig. 2. Ratio of the effective spin-lattice relaxation time, τ_1, to the effective spin-spin relaxation time, τ_2, versus the ratio of the "true" spin-lattice relaxation time, T_1, to the relaxation time for spin-exchange collisions, T_x.

28
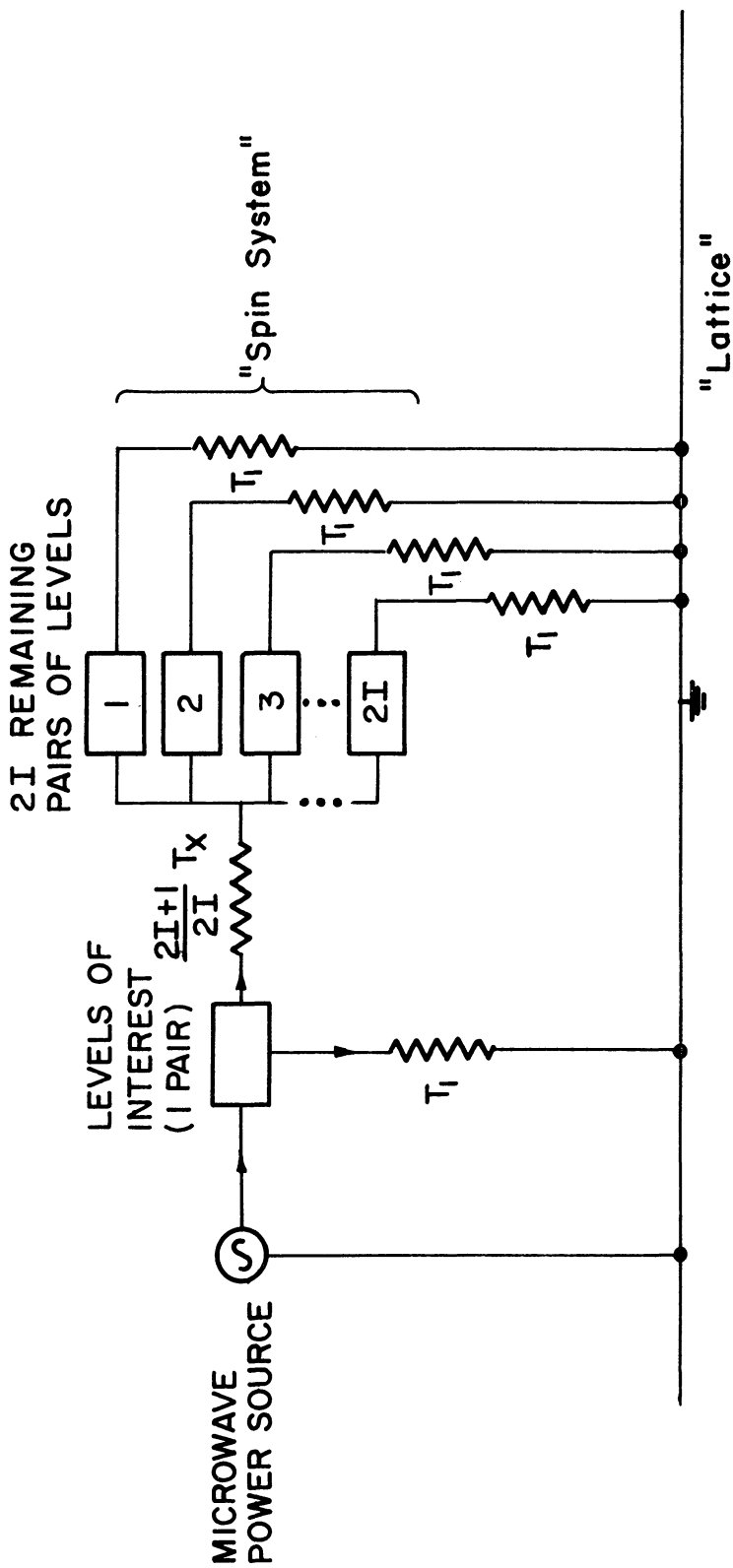
Fig. 3. An equivalent circuit for Eq. (II.34).

Here $1/\tau_2^*$ is the effective spin-spin relaxation rate due to the in-homogeneous field, $1/\tau_2$ is given by Eq. (II.34) and $1/\tau_2'$ is the measured relaxation rate. In a similar way, several distinct mechanisms may contribute to the spin-lattice relaxation rate, $1/T_1$. For example, both atom-atom collisions and collisions with the walls of a sample container will be present. The total relaxation rate is then given by

$$\frac{1}{T_1} = \frac{1}{T_1^*} + \frac{1}{T_w} \tag{II.39}$$

where $1/T_w$ is the collision rate with the container walls and $1/T_1^*$ an atom-atom collision rate.

Equation (II.37) forms the basis for the measurements to be discussed in the next chapter. There a simple modification of that formula which arises because of the experimental technique will be discussed. The formulae which support (II.37) apply only when the magnetic field H_0 is large. The problem is somewhat more complicated in case the Zeeman and hyperfine interactions are comparable. The solution of this intermediate field problem is relegated to the Appendix.

CHAPTER III

EXPERIMENTAL PROCEDURE AND RESULTS

A. DESCRIPTION OF APPARATUS

A functional diagram of the microwave spectrometer and associated electronics is shown in Fig. 4. The relationship between the displayed signal voltage and the microwave power absorbed by the sample has been examined in detail by many authors.[23,12] The following is a list the salient features of the apparatus.

1. The A.F.C. system stabilizes the spectrometer against small frequency changes and in doing so suppresses any dispersive components in the signal (i.e., χ'). A resonance spectrum is obtained by slowly varying the magnetic field.

2. Crystal detector bias is obtained directly from the klystron by shunting a small amount of power around the microwave bridge (sometimes called homodyning). This is in contrast to the more usual practice of introducing a slight unbalance in the bridge by means of the adjustable cavity iris. The homodyne system has the advantage of extending the system linearity to very low power levels, on the order of 5 micro-watts in the present design.

3. The microwave cavity (Fig. 4) used in this work resonates in the TE_{104} mode at a frequency of about 9.2 kmc/sec. The loaded Q of the cavity is nominally 1500. Quartz dewars are located in the cavity to position a paramagnetic sample in the maximum microwave magnetic field and to allow temperature control of the alkali sample and standard sample.

4. The spectrometer employs high frequency amplitude modulation of the magnetic field and phase sensitive detection. In this work the modulation frequency is 100 kc/sec. The displayed signal is in the form of the <u>derivative</u> of the absorption profile.
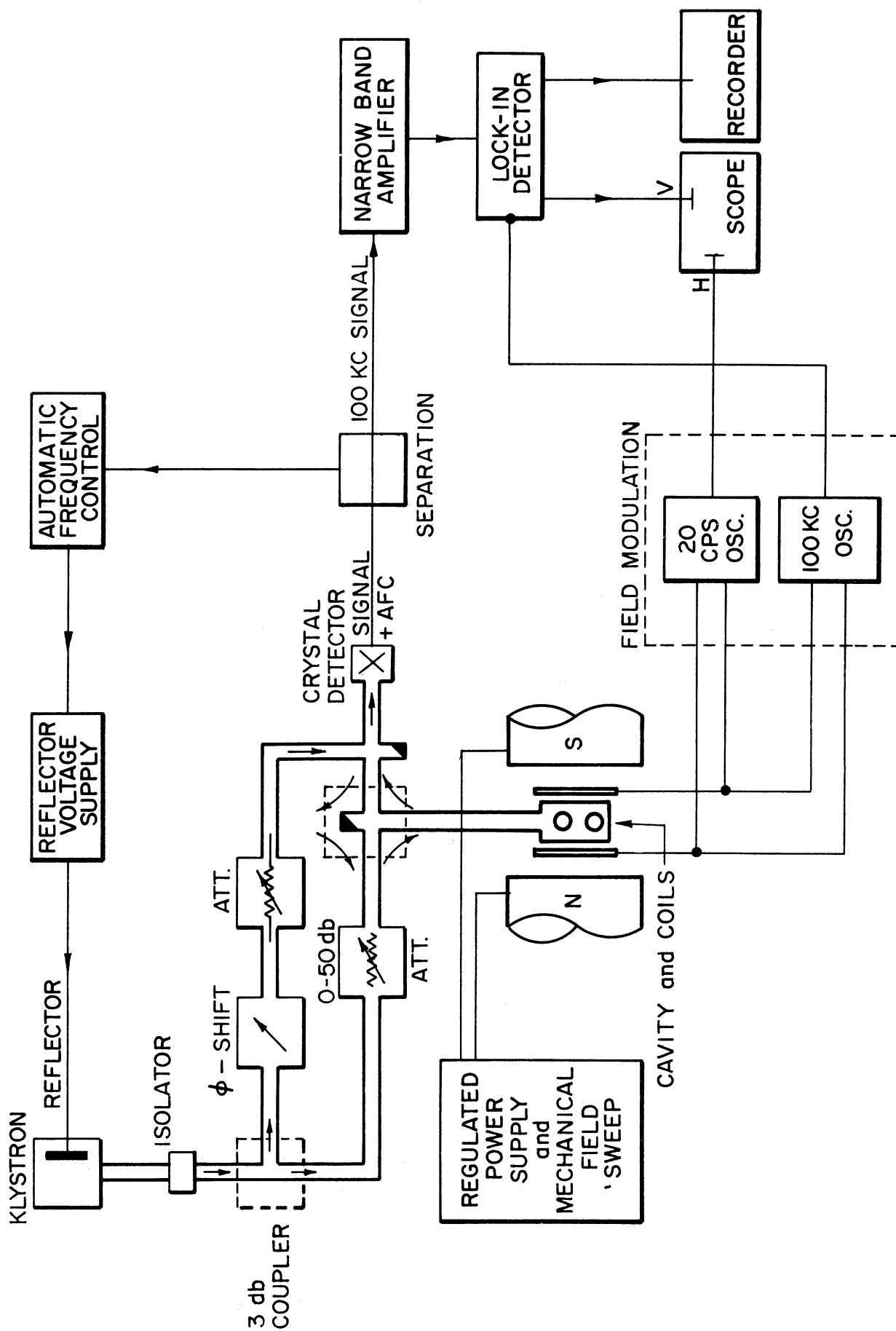
Fig. 4. Block diagram of the EPR spectrometer.

Moos[12] and others[24] have given formulas relating the signal voltage

at the recorder to the parameters of the spectrometer and paramagnetic

sample. A typical recorder tracing, in this case one of the resonance

lines observed in potassium, is shown in Fig. 5. If ΔV is the peak to

peak voltage difference on the recorder, one obtains[12]

$$\Delta V = A \frac{\delta^2 N}{(2I+1)(2S+1) T} \frac{\eta H_m^{eff}}{(\partial \omega_0 / \partial H)(\Delta H)^2} \qquad (III.1)$$

where $\gamma = 2\langle i|\mu_x|j\rangle/h$, N is the number of unpaired spins per unit

volume and T the absolute temperature. The filling factor η is given by

$$\eta = \frac{\int_{SAMP} H_1^2 dV}{\int_{CAV} H_1^2 dV} \qquad (III.2)$$

where $2H_1(x) \cos\omega t$ is the microwave magnetic field in the cavity.

Similarly, $H_m \cos\omega_m t$ is the modulation applied to the dc magnetic field

and

$$H_m^{eff} = \frac{\int_{SAMP} H_m H_1^2 dV}{\int_{SAMP} H_1^2 dV} \qquad (III.3)$$

ΔH is the spectral line width, in gauss, measured between the

points of maximum slope on the absorbtion curve (Fig. 6). ΔH is re-

lated to $1/\pi T_2$, the line width in frequency units, by

$$\Delta H = \frac{2}{\sqrt{3}} \frac{1}{T_2 (\partial \omega_0 / \partial H)} \qquad (III.4)$$

where $\partial \omega_0 / \partial H$ is the slope of the transition frequency.*

---

*$(\partial \omega_0 / \partial H) = \gamma$ in strong magnetic fields, where the hyperfine levels of the alkali atoms diverge linearly with the field strength. If the Zeeman interaction is smaller than, or of the same order of magnitude as, the hyperfine interaction, magnetic dipole transitions involve both reorientation and changes in size of the dipole moment. $\partial \omega_0 / \partial H$ can be computed from the Breit-Rabi formulas for the energy. Further consideration of this intermediate field case is given in the Appendix.
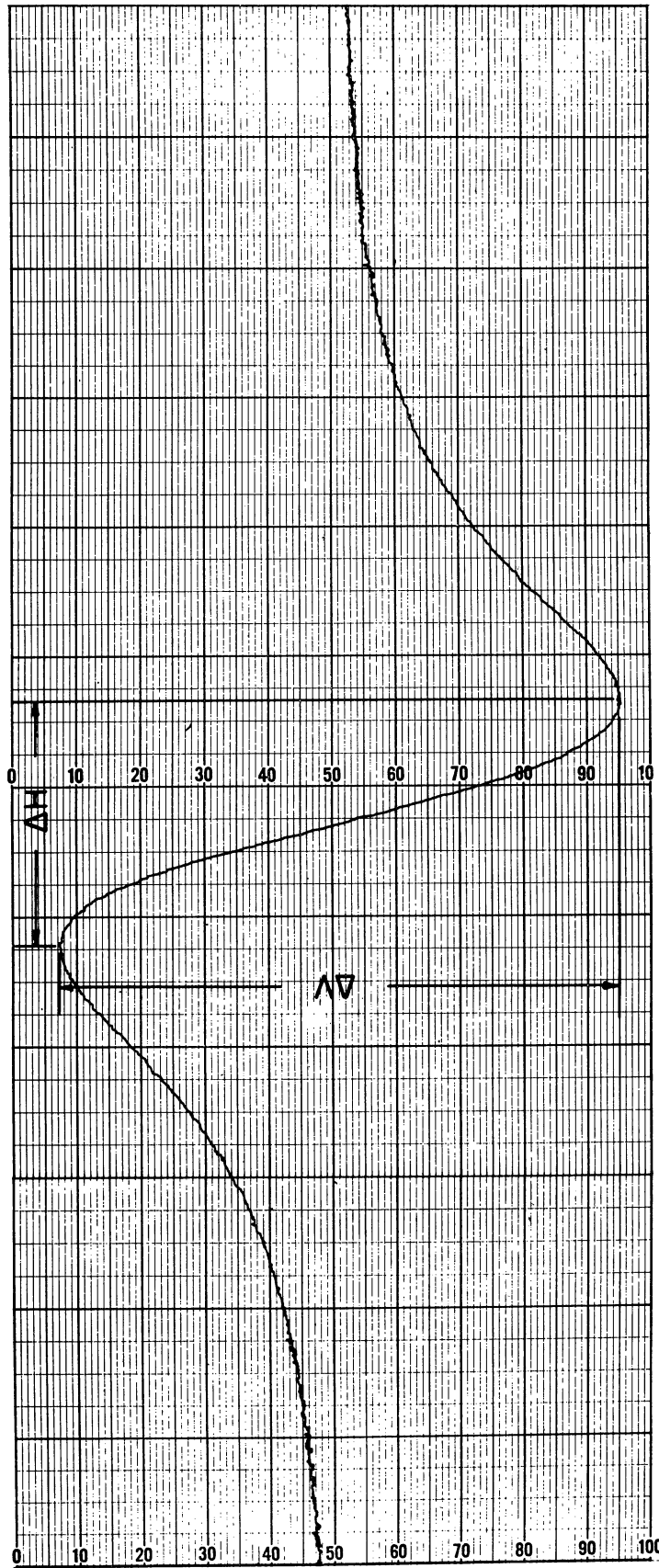
Fig. 5. Typical EPR spectrum of an alkali metal vapor (K^{39} shown).
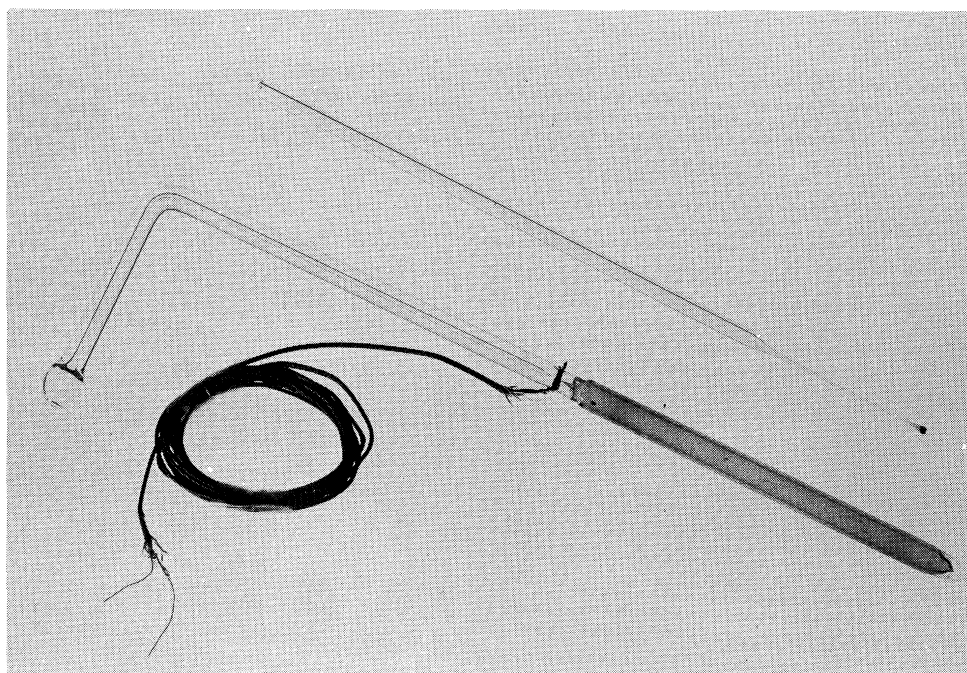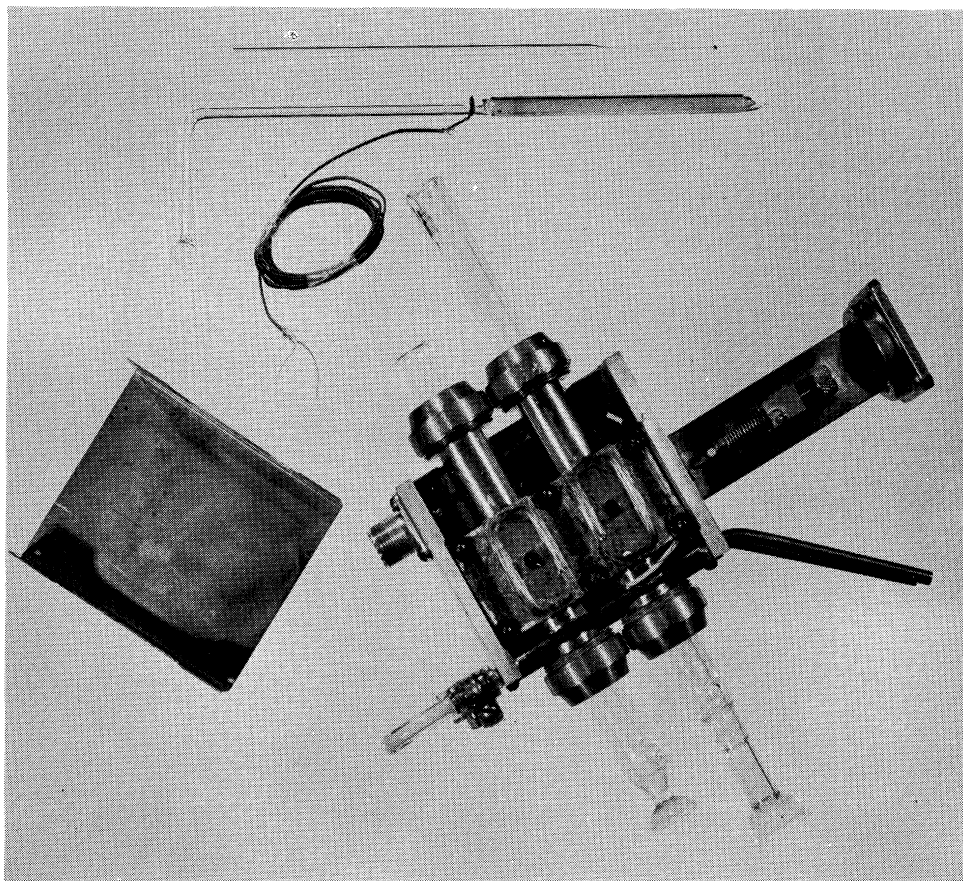
Fig. 6. Microwave cavity and sample tubes.

Equation (III.1) assumes that the saturation factor $\gamma^2 H_1^2 \tau_1 \tau_2 \ll 1$. The

factor A is a (known) constant incorporating the cavity Q, amplifier

gain settings, incident power, etc. More explicitly,

$$A = \beta G Q_L P_g$$

where β incorporates the conversion efficiency of the crystal detector

and power losses in the microwave bridge. β is a constant charac-

teristic of the spectrometer.

The experimental determination of the spin exchange cross section is

based on the two-fold application of Eq. (III.1): first, to the magnetic

resonance spectrum of the alkali metal vapors and to the particular

transition being studied there; and second, to the spectrum of Cu^{++} ions

in crystalline copper sulphate, $CuSO_4 \cdot 5H_2O$. In this experiment small

(1-2mg) single crystal specimens of copper sulphate were used to establish,

by direct comparison of signal voltages and line widths, the density N

of the alkali metal vapor at a given temperature.

B. EXPERIMENTAL PROCEDURE

Before proceeding to a discussion of the measurement technique

some understanding of the copper sulphate spectrum is needed, since

this material is to be used as a primary standard of intensity. The

lowest state of a free Cu^{++} ion is a ^2D state, corresponding to an

occupied 3d shell minus one electron. The effect of crystalline electric

fields and spin orbit coupling is to split the degeneracy of this state,

leaving behind as the lowest state a pair of levels which diverge

linearly in an applied magnetic field.[25] The next highest levels are

about 12000 cm^{-1} away and are not occupied at room temperatures.

Although there are two non-equivalent sites for the Cu^{++} ions in

the last lattice, a strong exchange interaction between the sites tends

to average out the spectral differences of the crystalline environments.

As a result the effective number of levels [previously $(2I+1)(2S+1)$] is

2 and a single spectral line is observed. However, the exchange inter-

action is sufficiently weak that the position and width of this line

depends on the orientation of the crystal axes with respect to the mag-

netic field. Associated with the two Cu^{++} sites in the lattice are two

crystalline (tetragonal) axes which are coplanar and nearly 90° apart.

The g-value for the dc magnetic field perpendicular to the plane of

these axes has been measured to be 2.09 ± 0.01, while in the plane of

the axes the g-value varies from 2.23 to 2.28.[25]

The particular usefulness of copper sulphate as an intensity

standard stems from the fact that the exchange narrowed spectrum has a

Lorentzian line shape,[26] and that the number of spins contributing to

the signal can be assayed by weighing the sample. The product $\Delta V(\Delta H)^2$,

which is a measure of the area under the absorbtion curve, may be

taken directly from recorder tracings for comparison with a similar

product for the alkali absorption curve. If the alkali and Cu^{++} signals

were not Lorentzian such a direct comparison would not be possible.

In practice small crystals of copper sulphate were selected and weighed on a microbalance. Typically these crystals weighed on the order of 1.5 mg, corresponding to 3.6×10^{18} spins. The crystals were affixed, with a small drop of Duco cement, to a thin Pyrex filament and a thin coating of paraffin applied to prevent the loss of waters of hydration. A crystal so mounted is shown in Fig. 4. A small piece of α-γ bisdiphenylene β-phenylallyl, which gives an intense and narrow signal at g=2, was attached to assist in locating the crystal in the maximum rf magnetic field in the cavity.

The crystals were oriented in the dc magnetic field so that the g-value in that direction was 2.09 ± 0.01. Thus $\partial\omega/\partial H$, in Eq. (III.1) is $2.09 \; \mu_0/\hbar$. The rf field, which is perpendicular to the dc field, then lies in the plane of the tetragonal axes. The g-value in that direction was taken to be 2.25 ± 0.03, so that $\gamma = 2.25 \; \mu_0/\hbar$. This orientation of the crystal corresponds to a minimum line width of about 30 gauss. It is also the orientation which gives the maximum signal to noise ratio.

The quantities $\partial\omega/\partial H$ and γ, as they pertain to the alkali spectra, are discussed in the Appendix. Table I presents a compilation of all the relevant matrix elements for the alkali transitions studied in this work, together with the data on the transitions studied by Moos.[12]

TABLE I

TABLE OF MATRIX ELEMENTS

Alkali	Transition	Field(Gauss)	γ*,**	$\partial\omega/\partial H$*
K^{39}	$(2,-1)-(2,-2)$	3360	$g\mu_0/\hbar$	$g\mu_0/\hbar$
Cs^{133}	$(4,-3)\leftrightarrow(4,-4)$	5790	$0.96g\mu_0/\hbar$	$0.92g\mu_0/\hbar$
	$(4,-2)\leftrightarrow(3,-3)$	4160	$0.82g\mu_0/\hbar$	$0.63g\mu_0/\hbar$
	$(4,-1)\leftrightarrow(3,-2)$	2480	$0.71g\mu_0/\hbar$	$0.37g\mu_0/\hbar$
Rb^{85+}	$(3,-1)\leftrightarrow(2,0)$	4100	$g\mu_0/\hbar$	$g\mu_0/\hbar$
Rb^{87+}	$(2,0)\leftrightarrow(1,-1)$	2900	$0.84g\mu_0/\hbar$	$0.69g\mu_0/\hbar$
Cu^{++}	---	3120	$2.25\ \mu_0/\hbar$	$2.09\ \mu_0/\hbar$

*For the alkali metals, g = 2.00.

**$g\mu_0/h$ = 2.80 M cps/gauss   [+]Reference 12

A typical alkali sample container is shown in Fig. 4. These samples were prepared by vacuum distillation of the metal into the containers. The sample tubes consist of precision bore (3/16" ± 0.002" I.D.) quartz tubing approximatly 2-1/2" long. Taking into account the variation in rf field strength over the length of the sample, the effective volume of the container is $0.51\ cm^3$. The tubing is sealed to a capillary quartz stem which leads to a small reservoir volume at the top of the sample (Fig. 4).

It had been intended that this thesis also include measurements on the exchange cross sections for Na.[23] However, because of the extreme chemical affinity of the hot sodium vapor for the walls of the sample tubes these measurements were not possible. Sodium transitions

were observed using small tubes made from special alkali-resistant glass (Schott No. 8243). These tubes lasted about 10 min, far too short a time for any measurements to be made. In addition, the dielectric loss of this glass is quite high and rather strongly temperature dependent. At the required operating temperatures ($\sim 400°C$) the Q of the cavity was reduced below operating limits.

The capillary and reservoir serve as a method of gettering impurities introduced when the sample tube is sealed off from the vacuum system. Although the pressure was never larger than 10^{-4} torr at the time of tip-off, without the capillary and reservoir of cold alkali metal it was found that the pressure in the sample tube subsequently rose as high as 10^{-2} torr. The exact nature of these impurity gases is unknown but their presense is felt since they can, and do, provide relaxation collisions which broaden the alkali spectrum. The impurities are apparently gettered by the cold alkali but are promptly released when the sample is heated to its operating temperature ($\sim 350°C$ in the case of potossium).

To produce a more permanent gettering action some of the alkali is moved through the capillary into the reservoir, which is located to one side of the axis of the bulb so as to be out of the stream of hot air blowing past. This metal remains relatively cool during an experimental run and, so long as the capillary remains open, effectively getters the impurities released by the hot alkali below. Using this technique the spin lattice relaxation time T_1 was increased, in

potassium, by as much as a full order of magnitude. Little, if any,

change was noted in the case of cesium, presumably because at the lower

temperatures employed for it the impurities were not released.

Experimentally, a copper sulphate crystal and alkali sample were

properly positioned in the two halves of the microwave cavity. An

additional piece of precision quartz tubing was slipped around the sul-

phate crystal to equalize the amounts of quartz in the two halves. This

was done to minimize any unwanted differences of the microwave field

distribution.

Hot air flowing past the alkali sample brought the alkali vapor

pressure to a point where detectable microwave absorption occurred. The

temperature was determined by a calibrated copper constantan thermo-

couple fastened to the outside of the sample tube. The temperature of

the copper sulphate crystal was determined by a thermometer before and

after an experimental run. Despite the presence of high temperatures

not more than 1 in. way, the temperature of the crystal was found to

remain nearly constant at about 30°C.

When the system had stabilized, the alkali resonance was located

and slowly scanned by varying the dc magnetic field. The field sweep

was provided by a motor driven Helipot potentiometer which added an

error voltage, varying linearly in time, to the reference voltage of

the magnet power supply. The sweep rate was determined, in units of

gauss per in. of recorder chart paper, by measuring the magnetic field

with a proton magnetic resonance probe. A similar procedure was followed

to obtain permanent records of the Cu^{++} spectrum. Also recorded on the chart paper was the amplifier gain settings, modulation amplitude, power incident on the cavity and the temperature of the alkali cell. Additional information on the details of the experimental procedure can be found in Reference 12.

C. RESULTS OF THE MEASUREMENTS

Equation (III.1) applies equally to the Cu^{++} and alkali resonances:

$$\Delta V_{ALK} = H' \frac{\gamma_A^2 \, N_A}{2 T_A (2I+1)} \frac{\eta_A \left(H_m^{eff}\right)_A}{\left(\frac{\partial \omega_0}{\partial H}\right)_A (\Delta H)_A^2}$$

$$\Delta V_{Cu} = H'' \frac{\gamma_{Cu}^2 \, N_{Cu}}{2 T_{Cu}} \frac{\eta_{Cu} \left(H_m^{eff}\right)_{Cu}}{\left(\frac{\partial \omega_0}{\partial H}\right)_{Cu} (\Delta H)_{Cu}^2}$$

The modulation coils shown on the cavity in Fig. 4 were especially constructed to provide as uniform modulation as possible over the active length of the alkali sample. Experimentally

$$\frac{\left(H_m^{eff}\right)_A}{\left(H_m^{eff}\right)_{Cu}} = 1.00 \pm 0.05$$

For the ratio of the filling factors we have

$$\frac{\eta_A}{\eta_{Cu}} = \frac{\frac{1}{2} \nu_A}{\nu_{Cu}}$$

where $v_A = 0.51 \text{ cm}^3$ is the active volume of the alkali sample. Thus

$$\frac{\Delta V_A}{\Delta V_{Cu}} = H''' \cdot \frac{T_{Cu}}{T_A} \cdot \frac{1}{2I+1} \cdot \frac{N_A \nu_A}{2 \, n_{Cu}} \cdot \frac{\gamma_A^2}{\gamma_{Cu}^2} \cdot \frac{\left(\partial \omega_0 / \partial H\right)_{Cu}}{\left(\partial \omega_0 / \partial H\right)_A} \cdot \frac{(\Delta H)_{Cu}^2}{(\Delta H)_A^2} \quad (III.5)$$

where $n_{Cu} = N_{Cu} v_{Cu}$ is the total number of copper ions. Using Eq. (III.5) the variation of the spectral line width of the alkali resonances with density was studied. In agreement with the theory of Chapter II, the

line width in all cases varied linearly with the density. The results

are shown in graphical form in Fig. 9.

It will be noticed that these plots do not extrapolate to zero

line width at zero density. This residual broadening may be attributed

to two effects: inhomogeneous magnetic fields in the gap of the elec-

tromagnet and relaxation collisions caused by collisions with the wall

of the sample tube and with impurity atoms. The magnet inhomogeneity

was approximately 50 milligauss over the sample.

The spin lattice relaxation time τ_1 was determined for cesium and

potassium by progressive saturation of the resonance. Making allowance

for the fact that the microwave field is distributed over the sample,

one finds [12]

$$\frac{\Delta V_1 \cdot V_2}{\Delta V_2 \cdot V_1} = \frac{1}{2}\left(\sqrt{1+\frac{3}{4}A'} + 1\right)^2 \left(\sqrt{1+\frac{3}{4}A} - \frac{1}{2}\right) \qquad \text{(III.6)}$$

where $A = \gamma^2 H_1^2 \tau_1 \tau_2$. ΔV_1 and ΔV_2 are the peak to peak signal voltages

at two very different power levels $P_1 \alpha V_1^2$ and $P_2 \alpha V_2^2$, respectively. The

magnitude of H_1^2 could be determined either from the measured Q of the

cavity* or by the saturation of a substance with known τ_1.** Both methods

*For a rectangular cavity operating in a TE_{IMN} mode, the relationship
 between the loaded Q of the cavity, Q_L, and the magnetic field
 strength H_1 (gauss), is

$$H_1^2 = 8 \times 10^7 \cdot \frac{P_g Q_L}{\nu_0 V_c} \cdot \frac{1}{1+(\%_n A)^2}$$

where P_g is the power incident on the cavity, ν_0 the resonant frequency
and $V_c = A \times B \times C$ is the cavity volume. C is the length of the cavity in
the direction of propagation (Z-direction) and A is the heighth of the
cavity.

**Small samples of the free radical α,γ-bisdiphenylene-β-phenylallyl
are very useful for this purpose. This substance is characterized by
$\tau_1 = \tau_2$ and a line width $\Delta H \sim 1/2$ gauss. It is easily saturated.

were used. Numerical values of T_1 and T_x were obtained by use of

Eq. (II.34). The relaxation measurements were subject to rather

large experimental errors, primarily due to fluctuations in the

cavity Q during an experimental run and uncertainties on the order

of 20% in H_1^2. Nevertheless, these measurements did show that for

line widths $\Delta H \gtrsim .2$ gauss, the spin lattice relaxation made a con-

tribution to the total line width no larger than 20%. For potassium,

this was true only if the self-gettering bulbs shown in Fig. 4 were

used.

Measurements on a typical sample bulb of potassium (the bulb was

of the type shown in Fig. 4) are summarized in Fig. 6. Plotted there

is the ratio of the measured relaxation times, τ_1/τ_2, versus $1/\tau_2$.

Throughout this experiment a lower limit to the usable line width was

set by the inhomogeneity in the magnetic field produced by the large

electromagnet (Fig. 3). The data plotted in Fig. 7 has been corrected

for a field inhomogeneity of 0.05 gauss, distributed over the volume

of the sample. This correction was characteristic of the Varian 6"

magnet (ring-shimmed) used in this work. Using Eq. (II.38)

$$\frac{1}{T_2} = \frac{1}{T_2'} - \frac{1}{T_2^*}$$

with

$$\frac{1}{T_2^*} = \gamma \Delta H \frac{\sqrt{3}}{2}$$

$\Delta H = 0.05$ gauss is the line width due to inhomogeneous fields and

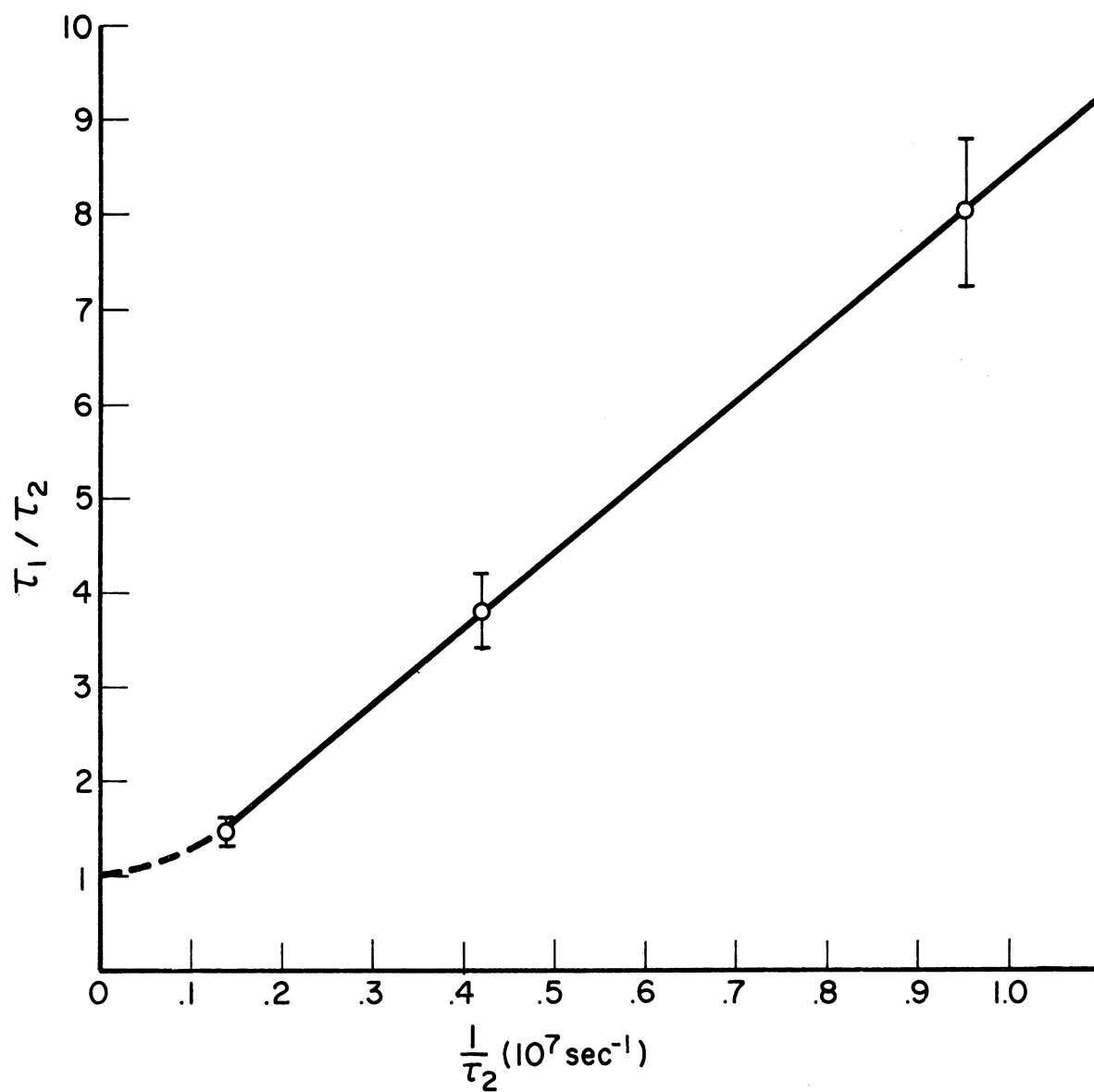$\gamma/2\pi = 2.8$ Mc/gauss is the gyromagnetic ratio for the potassium spins.

Fig. 7. Relaxation measurements on potassium: τ_1/τ_2 versus $1/\tau_2$.

By means of Fig. 2, or, equivalently, Eqs. (II.34), one obtains

the ratio T_1/T_x, which has been plotted versus $1/\tau_2$ in Fig. 8. One

sees from this graph that for narrow lines $(1/\tau_2$ small) the spin-

lattice relaxation is beginning to contribute significantly to the

observed line width. This means that as the vapor density is reduced

the rate of atom-atom collisions (and hence the exchange rate) gradually

loses out to the various T_1-processes. In particular, the life time

in a given spin state is determined, in this limit, by collisions with

the walls of the sample tube.

For a line width of 0.1 gauss $(1/\tau_2 = 1.5 \times 10^6 \sec^{-1})$ one estimates

from Fig. 8 that $T_1/T_x \simeq 2$. From Eq. (II.34), one finds

$$\frac{1}{T_2} \sim \frac{5}{2} \frac{1}{T_1}$$

or

$$T_1 = 1.6 \times 10^{-6} \sec.$$

On the other hand, if wall collisions are the dominant spin-lattice

relaxation mechanism $(T_1 \simeq T_\omega)$, the relaxation rate can be estimated

from elementary kinetic theory. Because of their exposure to a resonant

microwave field the atoms in the sample tube are not distributed accord-

ing to a Boltzmann distribution over the spin states. Instead, the

atoms have absorbed a small amount of energy from the microwave field.

In the steady state the rate at which energy is absorbed may be equated

to the rate at which this energy is removed by means of wall collisions.

In this experiment, the sample tubes are cylindrical, about 2-3 in. long

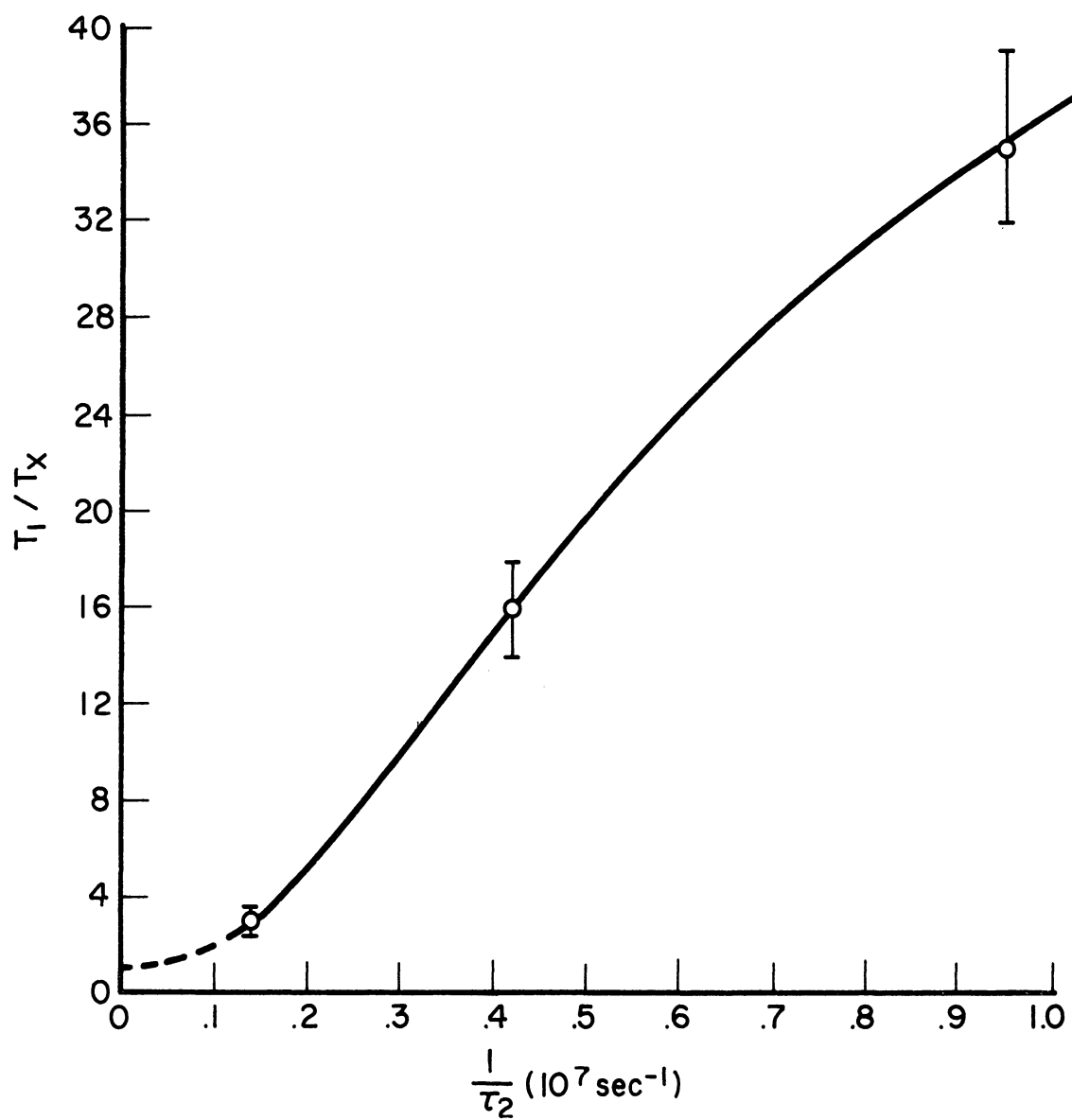and about 3/16 in. diameter. Neglecting end effects, the average time

Fig. 8. Relaxation measurements on potassium: T_1/T_x versus $1/\tau_2$.

between wall collisions is

$$\tau_w = D/\bar{v}$$

where D is the diameter of the sample tube and $\bar{v}$ the average speed of

the atoms.* For potassium at 300°C, $\bar{v} \simeq 5.7 \times 10^4$ cm/sec. This gives

$$\tau_w \simeq 8 \times 10^{-6} \; sec.$$

Although this estimate of the wall-time is perhaps the shortest

that can be expected, the agreement with the measured relaxation rate

is considered good. It is conceivable that additional relaxation

mechanisms are at work here but their appearance is masked by the

large experimental error.

The spin-exchange cross section Q_x can be related to the slope

$\delta\Delta H/\delta N$ (Fig. 9) through Eqs. (II.30), (II.34) and (III.4).

$$Q_x = \frac{1}{2}\sqrt{\frac{3}{2}} \; \frac{2I+1}{2I} \; \frac{(\partial\omega_0/\partial H)}{\bar{v}} \; \frac{\delta(\Delta H)}{\delta N} \tag{III.7}$$

$\bar{v}$, the average speed of the alkali atom at temperature T, was cal-

culated from standard kinetic theory. The quantities entering into

Eq. (III.7), together with the calculated cross sections, are given

in Table II.** Also included are the experimental results obtained

by Moos[12] on Rb^{85} and Rb^{87}.

---

*$\bar{v} = \sqrt{\dfrac{8KT}{\pi m}}$.

**$\partial\omega/\partial H$ is given in Table I, page 38.

$\triangle : K^{39} \underline{\quad \delta(\Delta H) \quad} = 0.059 \text{ per } 10^{15} \text{atoms}$
δN_A

$O : Cs^{133} \underline{\quad \delta(\Delta H) \quad} = 0.055 \text{ per } 10^{15} \text{atoms}$
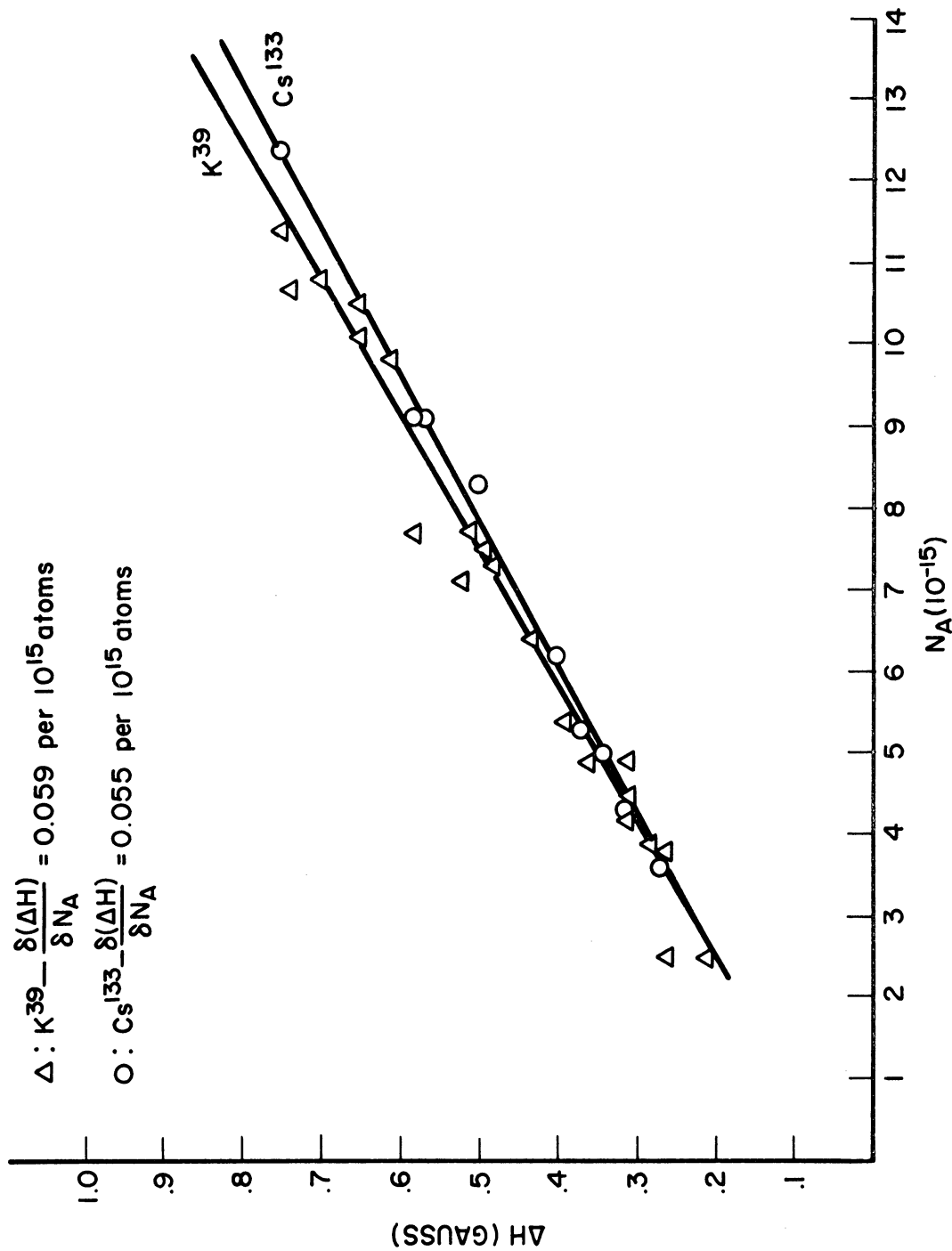δN_A

Fig. 9. Experimental results: Peak to peak line width versus alkali density.

TABLE II

EXPERIMENTAL RESULTS

Species	T°K	$\bar{v}$(cm/sec)	$\delta\Delta H/\delta N$(gauss/10^{16} atoms)	Q_x(cm^2)
K^{39}(I=3/2) (2,-2)↔(2,-2)	650	$5.9_2\times10^4$	0.60	$1.4_5\times10^{-14}$
Rb^{85}(I-5/2) (3,-1)↔(2,0)	550	$3.6_8\times10^4$	0.68*	$2.3_8\times10^{-14}$*
Rb^{87}(I=3/2) (2,0)↔(1,-1)	550	$3.6_8\times10^4$	0.98*	$2.6_3\times10^{-14}$*
Cs^{133}(I=7/2) (4,-2)↔(3,-3)	550	$2.9_6\times10^4$	0.58	$2.1_6\times10^{-14}$**

*Reference 12
**See Appendix (Part B) for a discussion of corrections which apply
  to the intermediate field case.

D. ERRORS

An extensive discussion of experimental errors has been given by

Moos.[12] In the present work only minor improvements were made in the

apparatus, none of which significantly affected the resultant error-

in-measurement. Most certainly the most important error arises from

improper positioning and orientation of the small copper sulphate in-

tensity standards. Within a given run the scatter of data points is

relatively small and random, but a large variation in slope can easily

arise from the systematic mis-orientation of the sulphate crystals.

Great care was taken to minimize this possibility.

After taking account of other sources of error, such as variation in temperature of the sulphate crystals, inaccuracies in field sweep calibration, distortions in the microwave field due to the quartz dewars and thin metal films within the sample tubes, etc.,[12] the cross sections quoted in Table III are assigned a 70% probable error of ±20%.

TABLE III

SOURCES OF ERROR IN THE DETERMINATION OF THE EXCHANGE CROSS SECTION

Source	Size
Random	±10%
Effect of films and quartz tubing	± 5%
Calibration of field sweeps	± 2%
Measurement of temperatures	± 2%
Copper sulphate line shape	–10%
Determination of sample volume	± 5%
γ and $\partial_{\omega}/\partial H$ for $CuSO_4 \cdot 5H_2O$	± 5%
Determination of $H_M(eff)$	± 5%
Miscellaneous	± 5%

Table IV (see Appendix) presents a compilation of the sources of error, together with the probable error assigned to each. Only a brief discussion of these errors will be given here; for a detailed discussion the reader is referred to the thesis by Moos.[12]

The copper sulphate crystals used in this work introduce two important sources of error. Because of a slight mis-orientation of the crystals in the microwave field the quantities γ_{cu}^2, $\partial\omega/\partial H)_{cu}$ and $(\Delta H)_{cu}$, all appearing in Eq. (III.5), acquire a corresponding variation. Assuming a $\pm 10°$ tilt in the crystal axes, the quantity $\gamma_{cu}^2/\partial\omega/\partial H)_{cu}$ is assigned probable error of $\pm 5\%$. $(\Delta H)_{cu}$, the peak-to-peak line width, was measured with an accuracy of $\pm 2\%$. Calibration of the mechanical field sweep was carried out with a proton magnetometer and frequency counter. Care was taken to always use the central position of the motor-driven potentiometer in the field sweep unit. This minimized the nonlinearities in the circuit.

Spectral line shapes are an important parameter in this experiment. Both the alkali metals and copper sulphate are expected to show Lorentzian line shapes. In the case of the alkali metal vapors the Lorentzian line shape follows from the assumption of collision broadening, whereas for copper sulphate this line shape is a consequence of a rather pronounced exchange narrowing. The importance of the spectral line shape lies in the fact that the number of atoms contributing to a signal is proportional to the total area under the absorption curve. For a Lorentzian line shape approximately 80% of this area lies within three line widths (peak-to-peak) of the center of the absorption. This means, for example, that if the absorption dropped more rapidly than a Lorentzian, at points removed by more than three line widths from the

center, one would have <u>under</u> <u>estimated</u> the spectral intensity by some 20%, which has the effect of increasing the computed cross sections by the same amount.

Careful measurements of the spectral line shape of copper sulphate and the alkali gases, show that the line shapes are quite accurately Lorentzian out to a least three line widths. A reasonable estimate of the uncertainty in the density measurements, due to deviations from the assumed line shapes, is ~10%.

Temperature measurements on the alkali samples were made by means of a copper-constantan thermocouple and precision potentiometer. The thermocouple was located outside the cavity but adjacent to the small puddle of alkali metal which was feeding vapor to the sample bulb below (Fig. 5). The temperature of the copper sulphate crystals was measured with a mercury thermometer. Good thermal shielding of the sulphate crystals was provided by the quartz dewar around it. Water cooling of the cavity also reduced the heat transfer. The extreme error associated with these temperature measurements is taken to be ±3%.

Having the source of vapor located downstream in the flow of hot air past the sample tube minimized the formation of thin metal films on the tube walls. However, occasionally the molten metal would break away and fall into the microwave cavity. This had the effect of immediately lowering the cavity Q and terminating that portion of the run. The sample tube was removed and the alkali metal restored to the top of the tube by heating in a Bunsen flame. After placing the tube

back in the cavity and awaiting the return of thermal equilibrium, the run could be resumed.

The measurement procedure entails the comparison of signals obtained from different absorbing samples located in each half of the same microwave cavity. An accurate comparison of signals requires the field distributions in the two halves be the same. This in turn requires that the symmetry of the cavity be maintained when the quartz sample tubes are inserted. For this reason a similar piece of quartz tubing was slipped around the copper sulphate crystal. It was found that the rf field intensity did not change by more than $\pm 5\%$ (probable error) when different sample tubes were used.

The field distribution within the cavity was probed by means of a small DPPH sample attached to a drawn out Pyrex fiber. When corrected for the (known) distribution of the modulation field, these measurements showed that the microwave field distribution was the theoretical distribution, except in the vicinity of the "chimneys" (Fig. 5). There, the fields were perturbed somewhat and penetrated the opening at the base of the chimney. These fringing fields were taken into account in the determination of the alkali sample volume. The probable error associated with the determination of the sample volume, and $H_m(eff)$, is $\pm 5\%$.

APPENDIX: ADDITIONAL COMMENTS ON THE DENSITY MATRIX TREATMENT

Certain features of the density matrix treatment given in Chapter II need further discussion. In Section A of this appendix the off-diagonal matrix elements corresponding to spin-states which are not resonantly coupled to the microwave field are shown to be unimportant, so long as the spin states are well resolved. In Section B approximate solutions to the equation of motion are obtained for the case of intermediate field strength (hyperfine coupling on the order of or less than the Zeeman interaction).

A. OFF-DIAGONAL MATRIX ELEMENTS

In Section C of Chapter II the equation of motion for the density matrix was solved with the assumption that only two off-diagonal matrix elements were nonvanishing. These matrix elements corresponded to the excitation of a given pair of energy levels by a microwave field. It is not necessary to retain this assumption, although under the conditions of the present experiment it is justifiable. The justification will now be given.

For simplicity only the case $I = 1/2$ (hydrogen) will be considered in detail. The states are labelled in order of decreasing energy; that is, $\alpha e \alpha n = 1$, $\alpha e \beta n = 2$, $\beta e \beta n = 3$ and $\beta e \alpha n = 4$. With this labeling, and for magnetic dipole transitions $\Delta M_S = \pm 1$, $\Delta M_I = 0$, the density matrix has the form

$$\rho = \begin{pmatrix} \rho_{11} & 0 & 0 & \rho_{14} \\ 0 & \rho_{22} & \rho_{23} & 0 \\ 0 & \rho_{32} & \rho_{33} & 0 \\ \rho_{41} & 0 & 0 & \rho_{44} \end{pmatrix}$$

Using this density matrix and Eq. (II.19) one finds

a. The diagonal matrix elements of ρ^c are unaffected by this new form, (i.e., the ρ^c_{ii} are still given by the expressions in Chapter II).

b. The off-diagonal elements are altered and, in the present notation, are given by

$$\rho^c_{14} = \rho^{c*}_{41} = \rho_{14} - \sin^2\frac{\phi}{2}\{1 - (\rho_{11} + \rho_{44})\}\rho_{14}$$

$$- \frac{i}{2}\sin\phi\{Z - (\rho_{11} - \rho_{44})\}\rho_{14}$$

$$+ \sin^2\frac{\phi}{2}(\rho_{11} + \rho_{44})\rho_{23} + \frac{i}{2}\sin\phi(\rho_{11} - \rho_{44})\rho_{23}$$

$$\rho^c_{23} = \rho^{c*}_{32} = \rho_{23} - \sin^2\frac{\phi}{2}\{1 - (\rho_{22} + \rho_{33})\}\rho_{23}$$

$$- \frac{i}{2}\sin\phi\{Z - (\rho_{22} - \rho_{33})\}\rho_{23}$$

$$+ \sin^2\frac{\phi}{2}(\rho_{22} + \rho_{33})\rho_{14} + \frac{i}{2}\sin\phi(\rho_{22} - \rho_{33})\rho_{14}$$

where $Z = \rho_{11} + \rho_{22} - \rho_{33} - \rho_{44}$ and $N = \rho_{11} + \rho_{22} + \rho_{33} + \rho_{44} = 1$.

Neglecting the very small frequency shift Δ (the expression for Δ is essentially unchanged, Eq. (II.35)) transforming to a coordinate system rotating with the sense of the Larmor precession at a frequency ω, the equations of motion assume the form

$$\dot{U}_A + \Delta\omega_A V_A = -\frac{1}{T_2} U_A + \frac{1}{T_x} U_B$$

$$\dot{U}_B + \Delta\omega_B V_B = -\frac{1}{T_2} U_B + \frac{1}{T_x} U_A$$

$$\dot{V}_A - \Delta\omega_A U_A = -\frac{1}{T_2} V_A + \frac{1}{T_x} V_B - \omega_1 Z_A$$

$$\dot{V}_B - \Delta\omega_B U_B = -\frac{1}{T_2} V_B + \frac{1}{T_x} V_A - \omega_1 Z_B$$

$$\dot{Z}_A - \omega_1 V_A = -\frac{1}{T_1} Z_A^0 - \frac{1}{T_2} Z_A + \frac{1}{T_x} Z_B$$

$$\dot{Z}_B - \omega_1 V_B = -\frac{1}{T_1} Z_B^0 - \frac{1}{T_2} Z_B + \frac{1}{T_x} Z_A$$

where $\Delta\omega_A = \omega_0^A - \omega$, $\Delta\omega_B = \omega_0^B - \omega$, $1/\tau_x = 1/2\tau_x$, $1/\tau_2 = 1/2\tau_x + 1/\tau_1$.

Also, U and V are the out of phase and in phase components of the

magnetization in the rotating frame, respectively. Z is the component

of magnetization along the applied field (Chapter II). These equations

represent the motion of two spins systems (A and B) in "magnetically

different environments" exchanging magnetization at the rate $1/\tau_x$.

Similar equations have been proposed by McConnell* in order to deal

with a similar problem in nuclear magnetic resonance.

The approximations made in Chapter II are represented by the

equations $V_B = U_B = 0$. The problem now is to determine under what

conditions these approximations are valid. A general solution will

not be attempted. Instead, only the case of relatively weak microwave

excitation will be treated (i.e., no saturation). For sufficiently

weak rf $Z_A \simeq 1/2 Z_0$, where $Z_0 = Z_A^0 + Z_B^0$ is the total equilibrium

*H.M. McConnell, J. Chem. Phys. 28, 430 (1958).

magnetization. Defining $G_A = U_A + iV_A$ and $G_B = U_B + iV_B$, the first

four equations of motion can be combined to give, in **steady state**,

$$\left\{\frac{1}{T_2} - i\Delta\omega_A\right\}G_A = \frac{1}{T_x}G_B - i\frac{1}{2}\omega_1 Z^0$$

$$\left\{\frac{1}{T_2} - i\Delta\omega_B\right\}G_B = \frac{1}{T_x}G_A - i\frac{1}{2}\omega_1 Z^0$$

These equations can in turn be combined to yield

$$\lambda_B G_B + \frac{1}{T_x}G_B = \lambda_A G_A + \frac{1}{T_x}G_A$$

whence

$$G_B = G_A \frac{\lambda_A + \frac{1}{T_x}}{\lambda_B + \frac{1}{T_x}} \qquad \text{with} \qquad \lambda_b = \frac{1}{T_2} + i\Delta\omega$$

When the frequency of the microwave field is very near the resonant

frequency for system A (i.e., $\omega \simeq \omega_0^A$), then

$$\lambda_A \simeq \frac{1}{T_2}$$

$$\lambda_B \simeq \frac{1}{T_2} - i\left(\omega_0^B - \omega_0^A\right)$$

Letting $1/\tau_2 + 1/\tau_x \equiv 1/\tau$ one finds

$$G_B \simeq G_A \frac{1}{1 + i\tau\left(\omega_0^B - \omega_0^A\right)}$$

Taking real parts this gives

$$U_B \simeq U_A \frac{1}{1 + \tau^2\left(\omega_0^B - \omega_0^A\right)^2} - V_A \frac{\tau\left(\omega_0^B - \omega_0^A\right)}{1 + \tau^2\left(\omega_0^B - \omega_0^A\right)^2}$$

Thus $U_B \ll U_A$ so long as $\tau^2\left(\omega_0^B - \omega_0^A\right)^2 \gg 1$. That is, $U_B = \chi_B''/2H_1 \simeq 0$

so long as

1. the resonances are well resolved: $\omega_0^B \gg \omega_0^A$

2. the effective exchange rate is small: $\tau \gg 1$

3. both 1 and 2 prevail.

The difference $\omega_0^B - \omega_0^A$ is easily calculated from the Breit-Rabi

formula for hyper-fine structure in a magnetic field. One finds,

in high field,

$$\left| \omega_0^B - \omega_0^A \right| = \hbar A$$

where A is hyperfine coupling constant. Since $1/\tau = 1/T_X$, in the

present case, the condition that only those off-diagonal matrix

elements are nonvanishing that correspond to levels nearly resonant

with the microwave field is

$$\hbar A \gg \frac{1}{T_X}$$

The case $I > 1/2$ yields this same condition. Of all the alkali

metals potassium (K^{39}) has the smallest hyperfine splitting

($\hbar A \simeq 4.6 \times 10^8$ cps). The measured exchange rates are on the order

of $1/T_X \sim 10^6$. Thus the approximations made in Chapter II are valid

to a very high degree.

B. INTERMEDIATE FIELDS

The equation of motion for the density matrix, though nonlinear,

is, in the so-called high-field case ($X \gtrsim 1$), separable and a steady

state solution readily found. However, in the weak or intermediate

field case ($X \lesssim 1$) the equations are nearly intractable and the

general steady state solution valid for all X has not been found.

The intermediate field case is of interest for two reasons. First,

the X-band microwave transitions in Cesium 133 and Rubidium 87 fall in

this region, and there is the possibility that in fields insufficient to decouple the electron and nucleus, the "effective" collision rate for spin exchange between specified energy states is thereby affected.

Second, even if residual hyperfine coupling is not important, the solution obtained in Chapter II must be corrected for the changes which occur in the magnitude of the dipole moment (i.e., γ) as the static field is lowered.

Although a complete solution to the intermediate field problem has not been obtained, still it is possible to examine the equations and show that when there is no saturation ($\omega_1 \ll 1$, $Z \simeq Z^0$) the effective spin-spin relaxation time is given by (II.34) to a very good approximation.

Information concerning the effects of hyperfine coupling is contained in the off-diagonal matrix elements of the density matrix. For $I = 1/2$, using the wave functions given by (II.27), and with the state labeling of Section I of this appendix, one calculates

$$\rho_{11}^c = \rho_{11} - \tfrac{1}{2}(1-z)\sin^2\tfrac{\psi}{2}\,\rho_{11} + \tfrac{1}{2}(1+z)\sin^2\tfrac{\psi}{2}\,A_0^2\,\rho_{44}$$
$$+ \tfrac{1}{2}(1+z)\sin^2\tfrac{\psi}{2}\,B_0^2\,\rho_{22}$$

$$\rho_{22}^c = \rho_{22} - \tfrac{1}{2}\sin^2\tfrac{\psi}{2}\left\{\tfrac{3}{2}\rho_{22} - \tfrac{1}{2}(A_0^2 - B_0^2)\rho_{22} - (A_0^2 - B_0^2)\rho_{22}z\right\}$$
$$+ \tfrac{1}{2}(1+z)\sin^2\tfrac{\psi}{2}\,A_0^2\,\rho_{33} + \tfrac{1}{2}(1-z)\sin^2\tfrac{\psi}{2}\,B_0^2\,\rho_{11}$$
$$+ \sin^2\tfrac{\psi}{2}\,A_0^2\,B_0^2\,\rho_{44}$$

$$\rho_{33}^c = \rho_{33} - \tfrac{1}{2}\sin^2\tfrac{\psi}{2}(1+z)\rho_{33} + \tfrac{1}{2}(1-z)\sin^2\tfrac{\psi}{2}A_0^2\rho_{22}$$

$$+ \tfrac{1}{2}(1-z)\sin^2\tfrac{\psi}{2}B_0^2\rho_{44}$$

$$\rho_{44}^c = \rho_{44} - \tfrac{1}{2}\sin^2\tfrac{\psi}{2}\left\{\tfrac{3}{2}\rho_{44} - \tfrac{1}{2}(B_0^2-A_0^2)\rho_{44} - (B_0^2-A_0^2)\rho_{44}z\right\}$$

$$+ \tfrac{1}{2}(1-z)\sin^2\tfrac{\psi}{2}A_0^2\rho_{11} + \tfrac{1}{2}(1+z)\sin^2\tfrac{\psi}{2}B_0^2\rho_{33}$$

$$+ \sin^2\tfrac{\psi}{2}A_0^2B_0^2\rho_{22}$$

$$\rho_{14}^c = \rho_{41}^{c*} = \rho_{14} - \rho_{14}\sin^2\tfrac{\psi}{2}\left\{\tfrac{3}{4} + \tfrac{1}{4}(A_0^2-B_0^2) - \tfrac{1}{4}z(1-A_0^2+B_0^2)\right.$$

$$\left. - \tfrac{1}{2}A_0^2\rho_{44}(1+A_0^2-B_0^2) - A_0^2\rho_{11}\right\}$$

$$- \tfrac{i}{4}\rho_{14}\sin\psi\left\{z(1+A_0^2-B_0^2) - 2A_0^2(\rho_{11}-\rho_{44})\right\}$$

$$\text{with} \quad z = \rho_{11} + (A_0^2-B_0^2)\rho_{22} - \rho_{33} - (A_0^2-B_0^2)\rho_{44}$$

In these equations

$$A_0 = [\Lambda_0^2 + 1]^{-1/2}$$

$$B_0 = \Lambda_0[\Lambda_0^2 + 1]^{-1/2}$$

$$\Lambda_0 = -X + \sqrt{1+X^2}$$

$$X = g_s\mu_0 H_0/A$$

For the matrix elements of $[\mathscr{H},\rho]$ one finds

$$\langle 1|[\mathscr{H},\rho]|1\rangle = \tfrac{1}{2}g_s\mu_0 2H_1\cos\omega t\, A_0(\rho_{41}-\rho_{14})$$

$$\langle 4|[\mathscr{H},\rho]|4\rangle = -\tfrac{1}{2}g_s\mu_0 2H_1\cos\omega t\, A_0(\rho_{41}-\rho_{14})$$

$$\langle 1|[H,\rho]|4\rangle = \rho_{14}(E_1 - E_4) + \tfrac{1}{2}g_s\mu_0 2H_1 \cos\omega t \, A_0(\rho_{44} - \rho_{11})$$

$$\langle 4|[H,\rho]|1\rangle = -\rho_{41}(E_1 - E_4) - \tfrac{1}{2}g_s\mu_0 2H_1 \cos\omega t \, A_0(\rho_{44} - \rho_{11})$$

Defining $\quad \gamma = \dfrac{2}{\hbar}\langle i|\mu_x|f\rangle \quad$ where $\quad \mu_x = g_s\mu_0 S_x$

$$\gamma = \tfrac{1}{\hbar}g_s\mu_0 A_0$$

Also,

$$\gamma H_1 \equiv \omega_1 \qquad \text{and} \qquad E_1 - E_4 = \hbar\omega_0$$

The equation of motion can be written

$$\dot{\rho}_{11} = -i\omega_1\cos\omega t(\rho_{41} - \rho_{14}) - \tfrac{1}{T_2}(\rho_{11} - \rho_{11}^c) - \tfrac{1}{T_1}(\rho_{11} - \rho_{11}^0)$$

$$\dot{\rho}_{22} = -\tfrac{1}{T_2}(\rho_{22} - \rho_{22}^c) - \tfrac{1}{T_1}(\rho_{22} - \rho_{22}^0)$$

$$\dot{\rho}_{33} = -\tfrac{1}{T_2}(\rho_{33} - \rho_{33}^c) - \tfrac{1}{T_1}(\rho_{33} - \rho_{33}^0)$$

$$\dot{\rho}_{44} = i\omega_1\cos\omega t(\rho_{41} - \rho_{14}) - \tfrac{1}{T_2}(\rho_{44} - \rho_{44}^c) - \tfrac{1}{T_1}(\rho_{44} - \rho_{44}^0)$$

$$\dot{\rho}_{14} = -i\rho_{14}\omega_0 + i\omega_1\cos\omega t(\rho_{11} - \rho_{44}) - \tfrac{1}{T_2}(\rho_{14} - \rho_{14}^c) - \tfrac{1}{T_1}\rho_{14}$$

$$\dot{\rho}_{41} = i\rho_{41}\omega_0 - i\omega_1\cos\omega t(\rho_{11} - \rho_{44}) - \tfrac{1}{T_2}(\rho_{41} - \rho_{41}^c) - \tfrac{1}{T_1}\rho_{41}$$

For sufficiently low fields ($x \ll 1$), $A_0 \simeq B_0 \simeq 1/\sqrt{2}$ and $\rho_{ii} \simeq \rho_{ii}^0$. Then $Z \simeq Z^0 \simeq 0$ and

$$\dot{\rho}_{14} \simeq -i\rho_{14}\omega_0 + i\omega_1\cos\omega t(\rho_{11}^0 - \rho_{44}^0) - \tfrac{1}{T_2}(\rho_{14} - \rho_{14}^c) - \tfrac{1}{T_1}\rho_{14}$$

$$\dot{\rho}_{41} \simeq +i\rho_{41}\omega_0 - i\omega_1\cos\omega t(\rho_{11}^0 - \rho_{44}^0) - \tfrac{1}{T_2}(\rho_{41} - \rho_{41}^c) - \tfrac{1}{T_1}\rho_{41}$$

where

$$\rho_{14}^c = \rho_{41}^{c*} \simeq \rho_{14} - \tfrac{q}{8}\cdot\tfrac{1}{2}\sin^2\tfrac{\gamma}{2}\,\rho_{14}$$

So

$$\dot{X} \equiv \dot{\rho}_{14} + \dot{\rho}_{41} = -\omega_0 Y - \frac{1}{T_2'} X$$

$$\dot{Y} \equiv i(\dot{\rho}_{14} - \dot{\rho}_{41}) = \omega_0 X - 2\omega_1 \cos\omega t(\rho_{11}^0 - \rho_{44}^0) - \frac{1}{T_2'} Y$$

with

$$\frac{1}{T_2'} = \frac{9}{8}\left(\frac{1}{2T_x}\right) + \frac{1}{T_1}$$

These equations may be compared with Eqs. (II.33) and (II.34) of

the text. The effect of hyperfine coupling is exhibited by the factor

9/8 in the equation for the effective exchange rate. Over a wide

range of magnetic fields the effective exchange rate is essentially

unaffected by the hyperfine coupling, as this is represented in the

eigenfunctions.

Calculations of the sort described above have been carried out

for the transitions of interest in cesium and the results tabulated

below.

TABLE IV

CORRECTIONS TO THE CESIUM EXCHANGE CROSS SECTION

Transition	X	$\frac{1}{T_2} = \alpha\left(\frac{2I}{2I+1}\frac{1}{T_x}\right) + \frac{1}{T_1}$
$(4,-1)\leftrightarrow(3,-2)$	0.75	$\alpha=0.81$
$(4,-2)\leftrightarrow(3,-3)$	1.26	$\alpha=0.84_5$
$(4,-3)\leftrightarrow(4,-4)$	1.78	$\alpha=0.94$

With regard to changes that occur in the size of the magnetic

dipole moment in intermediate fields, one is required to use the

correct eigenfunctions. The gyro-magnetic ratio is $\gamma = 2/\hbar$

$< i \ |\mu_x| j >$, with $\mu_x = g_s\mu_o S x$. Then

$$\gamma = \frac{2g_s\mu_o}{\hbar} \langle FM | S_x | F'M' \rangle$$

$$= \frac{g_s\mu_o}{\hbar} A_M A_{M-1}$$

with $A_M = \lambda_M / \sqrt{\lambda_M^2 + \lambda_M^2}$. The quantities λ_M and Λ_M are given by

Eqs. (II.27a).

The mixing of the electron spin-states by the hyperfine inter-

action in intermediate fields leads, then, to three important correc-

tions to the high-field analysis (Chapter II).

1. Through $\gamma^2 = 2/\hbar \ | < i|\mu_x|f > |^2$ the transition probability for
magnetic dipole transitions between a given pair of energy
levels ($i \leftrightarrow f$) decreases with decreasing field strength.

2. In contrast to the behavior at high fields, the energy levels
in intermediate fields have curvature. Hence $\gamma \neq \partial_\omega/\partial H$ and
the relationship between line width measured in units of the
magnetic field (gauss) and line width measured in frequency
units is

$$\left[T_2(\sec) \right]^{-1} = \frac{2}{\sqrt{3}} \frac{\partial \omega}{\partial H} \left[\Delta H (gauss) \right]$$

3. In intermediate fields the connection between the spin-spin
relaxation time (τ_2) and the mean time between exchange
events (T_x) is not simple. _Assuming_ that the spin-lattice
relaxation (T_1) makes a negligible contribution to the line
broadening, the relationship is

$$\frac{1}{T_2} = \alpha \left[\frac{2I}{2I+1} \frac{1}{T_x} \right]$$

where α is a numerical correction factor arising from the complicated mixing of the electron spin-states. In this work the $(F, M_F) = (4, -2) \longleftrightarrow (F', M_F') = (3, -3)$ was used for the determination of an exchange cross section. For this transition, and for a value of $X = 1.26$ appropriate to the magnetic field used, the value of α is $\alpha = 0.84$. If this same transition had been studied in the high-field limit (K band microwaves), $\alpha = 1$.

There is, however, little experimental evidence that the numerical correction α, which should be applied to the line width data, is correct. In cesium there are three transitions which can be observed at X-band frequencies (9.3 KMC). With the cesium gas at constant temperature (constant density) the line widths of each of these transitions was measured. The results are summarized below.

TABLE V

LINE WIDTHS FOR VARIOUS TRANSITIONS IN CESIUM

Transition	ΔH	$\partial \omega / \partial H$	$1/\tau_2$	$\dfrac{1}{\alpha \tau_2} = \dfrac{2I}{2I+1} \dfrac{1}{T_x}$
(1):(4,-3)$\longleftrightarrow$(4,-4)	0.41	0.92 $g\mu_0/\hbar$	5.9×10^6	6.3×10^6
(2):(4,-2)$\longleftrightarrow$(3,-3)	0.50	0.63 $g\mu_0/\hbar$	4.8×10^6	5.7×10^6
(3):(4,-1)$\longleftrightarrow$(3,-2)	0.67	0.37 $g\mu_0/\hbar$	3.7×10^6	4.6×10^6
(1):(4,-3)$\longleftrightarrow$(4,-4)	0.35		5.0×10^6	5.3×10^6
(2):(4,-2)$\longleftrightarrow$(3,-3)	0.42		4.1×10^6	4.9
(3):(4,-1)$\longleftrightarrow$(3,-2)	0.55		3.1×10^6	3.8
(1):(4,-3)$\longleftrightarrow$(4,-4)	0.19		2.6×10^6	2.8
(2):(4,-2)$\longleftrightarrow$(3,-3)	0.25		2.4×10^6	2.9
(3):(4,-1)$\longleftrightarrow$(3,-2)	0.40		2.2×10^6	2.7

According to the theory the numbers in the far right hand column, being essentially the product of the density and the exchange cross section, should, at any given temperature, be the same for all three transitions. The agreement with theory is quite good for the narrower line widths but there is progressive deterioration of the agreement with increasing temperature.

The reason for this is not understood. It is possible that the contribution of the spin lattice relaxation to the line width is considerably more complex than Eqs. (II.34) might indicate. Although measurements of the spin lattice relaxation time (τ_1) showed that τ_1 was approximately the same for each of the transitions, one is not justified in merely subtracting out this (apparent) contribution to the line width. It is believed that the difficulty could be resolved if a complete numerical solution to the equations of motion for intermediate fields was available, including the effects of spin lattice relaxation.

The experimental value for the exchange cross section of cesium has been corrected by dividing the measured cross section by the factor $\alpha = 0.84$. This correction is the one appropriate to the $(4,-2) \leftrightarrow (3,-3)$ transition.

REFERENCES

1. Wittke, J. P. and Dicke, R. H., Phys. Rev. 103, 620 (1956).

2. Purcell, E. M. and Field, G. B., Astrophys. J. 124, 542 (1956).

3. Dehmelt, H. G., Phys. Rev. 109, 381 (1958) and J. Phys. et radium 19, 866 (1958).

4. For a review of optical pumping techniques see, for example, Skiotskii and Izyumova, Usp. Fig. Nauk. 73, 423-470 (1961) (Translation: Soviet Physics Uspelski 4, 177 (1961)).

5. Franken, P., Sands, R. H., and Habart, J. L., Phys. Rev. Letter 1, 52, 118 (1958).
   Novick, R. and Peters, H. E., Phys. Rev. Letters 1, 54 (1958).
   Anderson, L. N., F. M. Pipkin and G. Baird, Phys. Rev. 116, 87 (1959).

6. Bender, P., Phys. Rev., 132, 2154 (1963). (a) See also Hobart, J. L., Thesis, University of Michigan, 1962 (unpublished).

7. Kleppner, D., Goldenburg, H. M., and Ramsey, N. F., Phys. Rev. 126, 603 (1962).

8. Balling, L. C., Hanson, R. J., and Pipkin, F. M., Phys. Rev. 133, A607 (1964).
   Balling, L. C. and Pipkin, F. M., Phys. Rev. 136, A46 (1964).

9. For example, see Metals Reference Handbook, C. J. Smithells, ed., (Butterworth Scientific Publications, Ltd., London, 1955) Vol. II, p. 613. Also, Ditchburn, R. W. and Gilmour, J. C., Rev. Mod. Phys. 13, 310 (1941) and, Gran, G. G. and Schaefer, K. L., Landott-Bornstein Zahlenwerte (Springer-Verlag, Berlin, 1960) Vol. II, p. 7.

10. For example, see Anderson, L. W. and A. T. Ramsey, Phys. Rev. 124, 1862 (1961).

11. Jarrett, S. M., Thesis (University of Michigan, 1962).

12. Moos, H. W., Thesis (University of Michigan, 1961).

13. Moos, H. W. and R. H. Sands, Phys. Rev. 135, A591 (1964).

REFERENCES (Concluded)

14. Rosen, N. and Ikehara, S., Phys. Rev. $\underline{43}$, 5 (1933).

15. Slater, J. C., Phys. Rev. $\underline{36}$, 57 (1930).

16. Wu, Ta-Yon and Ohmura, To, Quantum Theory of Scattering (Prentice-Hall, Inc., New Jersey, 1962) p. 4.

17. Op. cit. p. 235.

18. D. Ter Haar, Reports Prog. Physics $\underline{24}$, 304 (1961).

19. Karplus, R. and Schwinger, J., Phys. Rev. $\underline{73}$, 1020 (1948).

20. Kopfermann, H., Nuclear Moments (Academic Press, Inc., New York, 1958), p. 26.

21. Abragam, A., Principles of Nuclear Magnetism (Oxford, 1961) p. 22.

22. Op. cit. p. 46.

23. Goldsbrough, J. P. and M. Mandel, Rev. Sci. Instr. $\underline{31}$, 1044 (1960).

24. Singer, L. S. and J. Kommondeur, J. Chem. Phys. $\underline{34}$, 133 (1961). Kumagai, H., et al., J. Phys. Soc. Jap. $\underline{9}$, 376 (1954).

25. Bagguley, D. M. S. and J. H. E. Griffiths, Proc. Roy. Soc. (London) A$\underline{201}$, 366 (1950).

26. Anderson, P. W. and P. R. Weiss, Rev. Mod. Phys. $\underline{25}$, 269 (1953).

27. Glossgold, A. E., Phys. Rev. $\underline{132}$, 2144 (1963). Also, Glossgold, A. E. and S. A. Lebedoff, Ann. Phys. $\underline{28}$, 181 (1964).

28. Theoretical discussions have also been given by, Mago, R. M., J. Chem. Phys. $\underline{34}$, 169 (1961). Glossgold, A. E. and S. A. Lebedeff, Ann. Phys. $\underline{28}$, 181 (1964). Smith, F. J., Planet. Space Sci. $\underline{11}$, 1126 (1963). Dalgarno, A., Proc. Roy. Soc. A$\underline{262}$, 132 (1961). Comparison of theory and experiment is based on data obtained by, Hildebrandt, A. F., F. B. Booth and C. A. Barth, J. Chem. Phys. $\underline{31}$, 273 (1959).